Predictive Current Control Strategy for Single Phase Grid Connected Inverter

Derar Ahmad Abdalatef Zedan

Submitted to the
Institute of Graduate Studies and Research
in partial fulfillment of the requirements for the Degree of

Master of Science
in
Electrical and Electronic Engineering

Eastern Mediterranean University
March 2014
Gazimağusa, North Cyprus

Approval of the Institute of Graduate Studies and Research

Prof. Dr. Elvan Yılmaz
Director

I certify that this thesis satisfies the requirements as a thesis for the degree of Master of Science in Electrical and Electronic Engineering.

Prof. Dr. Aykut Hocanın
Chair, Department of Electrical and Electronic Engineering

We certify that we have read this thesis and that in our opinion it is fully adequate in scope and quality as a thesis for the degree of Master of Science in Electrical and Electronic Engineering.

Prof. Dr. Osman Kükrer
Supervisor

Examining Committee

1. Prof. Dr. Osman Kükrer
2. Prof. Dr. Runyi Yu
3. Asst. Prof. Dr. Suna Bolat

ABSTRACT

In this thesis, the predictive current control method is employed to control the single phase grid connected inverter under the condition of known grid voltage and load current. In real implementation the controller needs a certain time to do the required digital sampling and computations before the control command proceed to the inverter switches. Traditional predictive current control use the previous switching interval values in order to predict the required average inverter output voltage to follow the reference current. Nowadays, the availability of fast and low cost digital signal processer boards (DSP's) makes the implementation of predictive controllers simpler and more sufficient, based on above an improved predictive current control algorithm is developed such that the inverter work with high performance.

An improved predictive current control algorithm is developed by setting the sampling point just ahead the controlling point by the period of total sampling and computation delay, this adjustment make the control approach more robust against the system parameter variation. Moreover, the grid voltage prediction using the linear sine wave prediction instead of the traditional linear extrapolation prediction is sufficient to give more enhancements to the injected power in the utility grid.

Keywords: predictive current control, single phase grid connected inverters, discrete time control, renewable energy.

ÖZ

Bu tezde, şebekeye bağlanmış tek faz bir evirgeçin, şebeke geriliminin bilinmesi durumu için, öngörücü akım denetim yöntemi kullanılmıştır. Gerçek uygulamada, denetim komutunun evirgeç anahtarlarına uygulanmasından önce, gerekli sayısal örnekleme ve hesaplamaların yapılabilmesi için denetleyicinin belli bir zamana gereksinimi vardır. Geleneksel öngörücü akım denetimi, referans akımının takip edilebilmesi için gerekli olan evirgeç ortalama çıkış gerilimini hesaplamak için bir önceki örnekleme aralığına ait değerleri kullanır. Günümüzde, hızlı ve düşük maliyetli sayısal işaret işlemcilerinin bulunabilirliği, öngörücü denetleyicilerin uygulanmasını basitleştirmiştir. Buna dayanarak, evirgeçin yüksek başarımlı çalışması için iyileştirilmiş bir öngörücü akım denetleyicisi geliştirilmiştir.

Bu denetleyicide örnekleme anı, toplam örnekleme ve hesaplama gecikmesine eşit bir zaman aralığı farkı ile denetleme anından önceye alınmaktadır. Bu ayarlama ile denetim yaklaşımı sistemin parametre değişimleri karşısında daha dayanıklı hale gelmesine yol açmıştır. Buna ek olarak, şebeke geriliminin öngörülmesi için, geleneksel doğrusal dışdeğerleme yerine sinüs dalga doğrusal öngörü kullanılarak şebekeye verilen gücün daha verimli olması sağlanmıştır.

Anahtar Kelimeler: Öngörücü akım denetimi, tek faz şebekeye bağlı evirgeç, kesik zamanlı denetim, yenilenebilir enerji.

To My Lovely Land Palestine

ACKNOWLEDGMENTS

At the outset, thank God Almighty, for the completion of this thesis. My deepest gratitude and appreciation goes to my great supervisor Prof. Dr. Osman Kukrer for his assistance and guidance in my research. This thesis would not be possible without Prof. Dr. Osman Kukrer.

Thanks to everyone who helped me to complete this thesis. Appreciations also goes to all academic staff at the Electrical and Electronic Engineering Department.

Special thanks go to my best friends Ahmad Yassen and Hamza Ahmad for their support in each moment I spend in North Cyprus.

Finally, I don't forget to give the precious and valuable thanks to my father, mother, brothers and sisters for their moral and financial support during all years of my study. I'm asking God to save them and give them care and health.

TABLE OF CONTENTS

LIST OF TABLES

LIST OF FIGURES

LIST OF SYMBOLS/ABBREVIATIONS

T_{period}	Switching Time Period
V_{grid}	GridVoltage
BJT	Bipolar Junction Transistor
CSI	Current Source Inverter
DSP	Digital signal processer
IGBT	Insulated-Gate Bipolar Transistor
IPCC	Improved Predictive Current Control
LSWP	Linear Sine Wave Prediction
MOSFET	Metal Oxide Semiconductor Field Effect Transistor
PCC	Predictive Current Control
SPWM	Sinusoidal Pulse Width Modulation
TPCC	Traditional Predictive Current Control

Chapter 1

INTRODUCTION

1.1 Renewable Energy

Traditional energy sources like natural gas, coal and oil are becoming unable to meet the growing demand of energy consumption. In addition to the fact that it is the main source of environmental pollution, it is not available in all countries and this availability is always in limited quantities for certain periods.

Renewable energy is defined to be the form of energy coming from any natural, uninterrupted and clean source, such as sunlight, wind, geothermal and waves. Nowadays all these sources can generate electricity using certain collectors, such as photovoltaic cells and wind turbine. But we cannot use this electricity directly because it is not regulated or not alternating current (AC). The form of the electricity should be an AC waveform, so that we can get benefit from it. To solve this obstacle, modern technologies have main contributions of their investments in the development of grid connected inverters.

From above, we consider the advantages and importance of renewable energy sources. But the question is how to employ the above mentioned sources to meet the

challenges of energy consumption. In this thesis, a method of current control for grid connected inverters is discussed.

1.2 Inverters

An inverter is a power electronics device which converts direct current (DC) to a symmetric alternating current waveform (AC). The resultant output can be variable voltage, variable frequency or variable phase angle according to load operation requirements. Figure 1.1 shows the general structure of a DC-AC converter.

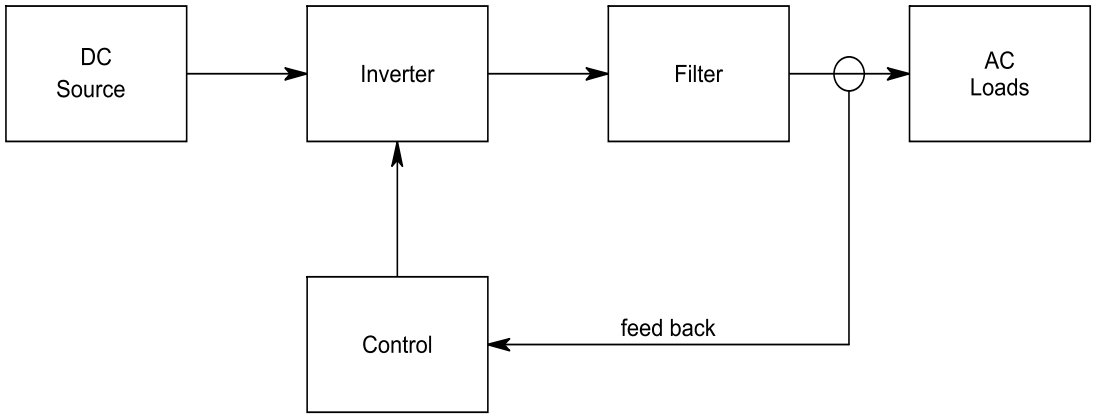

Figure 1.1: General structure of DC-AC converter [1].

In general, inverters are classified as voltage source inverter (VSI) and current source inverter (CSI). A voltage source inverter is widely used in low and medium power applications and fed from constant voltage source with negligible internal impedance. While a current source inverter is used in medium-voltage high-power applications and fed from constant current source with high impedance.

1.2.1 Single Phase Half Bridge Inverter

In a single phase half-bridge inverter, we need one leg of bidirectional switches. Each switch consists of a semiconductor device which may be a BJT, IGBT, or MOSFET connected to a diode in parallel. Figure 1.2.a shows the general structure

of a single phase half-bridge inverter. Figure 1.2.b shows the inverter output voltage and current waveforms.

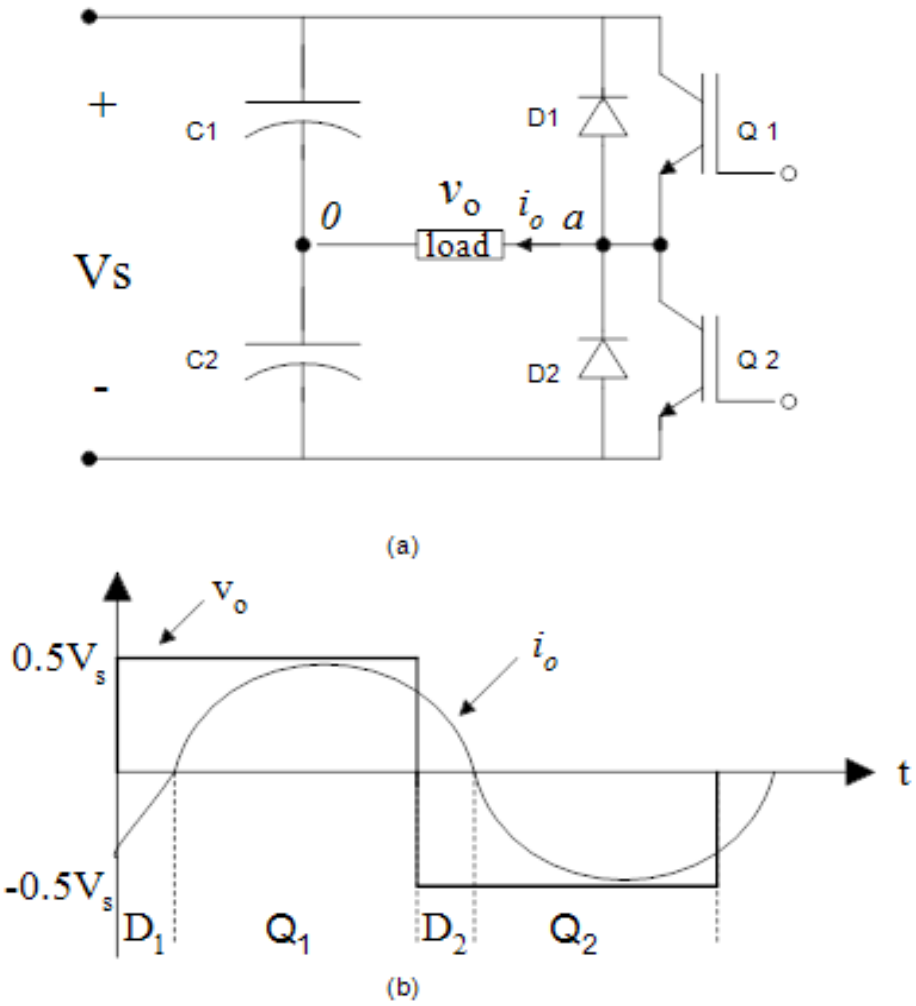

Figure 1.2: (a) Single phase half-bridge inverter. (b) Inverter output voltage and current waves [2].

Two equal capacitors C1 and C2 divide the DC source and give a center point 0. The switches Q1 and Q2 conduct in the first and in the second half cycles, respectively, producing voltage amplitudes $+\frac{V_s}{2}$ and $-\frac{V_s}{2}$. In the case of inductive load, D2 conducts when Q1 is turned off because the inductive load current cannot be interrupted immediately after the inverter output voltage changes. Similarly, D1

conducts when Q2 is turned off for the same reason. These diodes feed the power back to the DC source and are known as feedback or free-wheeling diodes .

1.2.2 Single Phase Full Bridge Inverter

In Figure 1.3.a a single phase full-bridge inverter is shown. The inverter consists of two legs, each leg having two power switches each with a diode in parallel. The diode is called free-wheeling diode, which allows the energy to return back to the DC source. When the transistors Q1 and Q2 are turned on, the power supply Vs is applied to the load. If transistors Q3 and Q4 are switched on, again the voltage of -Vs appears across the load. The output voltage and current waveforms will be as shown in Figure 1.3.b.

There are many switching states which can be considered for this case. All the possible switching states are shown in Table 1.1. The output voltage will be the positive source voltage $+V_s$ when Q1 and Q2 are ON and Q3 and Q4 are off. Similarly, the output voltage is $-V_s$ when Q3 and Q4 are on and Q2 and Q1 are off.

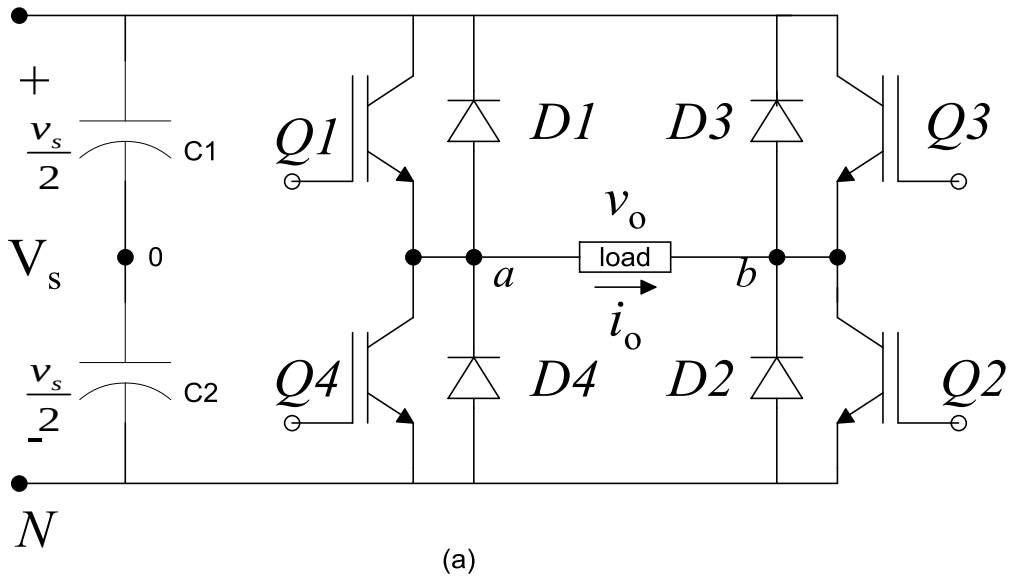

(a)

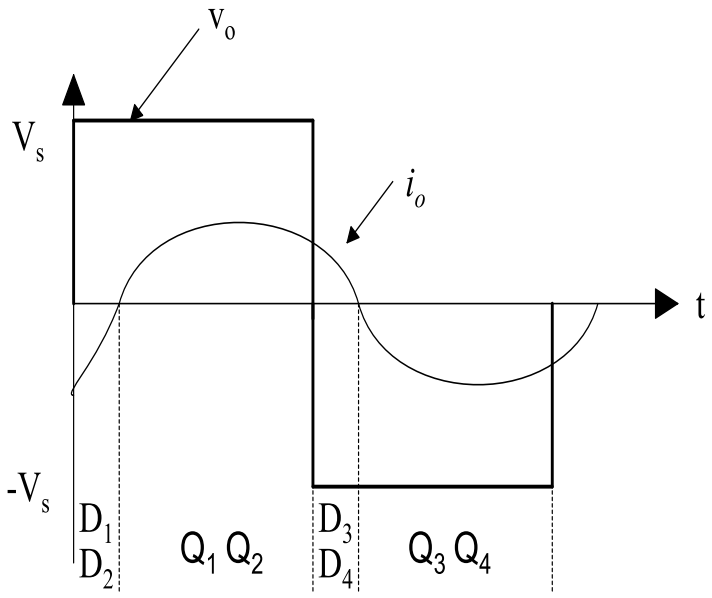

(b)

Figure 1.3: (a) single phase full bridge inverter, and (b) inverter output voltage and current waves [1].

Notice that, a zero output voltage appears on the load side when Q1 and Q3 are on and Q4 and Q2 are off or when Q4 and Q2 are on and Q1 and Q3 are off.

Table 1.1: Switching states of Single phase full bridge inverter.[1]

State	State No	Switch State	Vao	Vbo	Vo	Components Conducting
Q_1,Q_2 ON	1	1 0	$V_s / 2$	$-V_s / 2$	V_s	Q_1,Q_2 if $i_o > 0$
Q_4,Q_3 Off						D_1,D_2 if $i_o < 0$
Q_4,Q_3 ON	2	0 1	$-V_s / 2$	$V_s / 2$	$-V_s$	D_4,D_3 if $i_o > 0$
Q_1,Q_2 Off						Q_4,Q_3 if $i_o < 0$
Q_1,Q_3 ON	3	1 1	$V_s / 2$	$V_s / 2$	0	Q_1,D_3 if $i_o > 0$
Q_4,Q_2 Off						D_1,Q_3 if $i_o < 0$
Q_4,Q_2 ON	4	0 0	$-V_s / 2$	$-V_s / 2$	0	D_4,Q_2 if $i_o > 0$
Q_1,Q_3 Off						Q_4,D_2 if $i_o < 0$
Q_1,Q_2 Off	5	off	$-V_s / 2$	$V_s / 2$	$-V_s$	D_4,D_3 if $i_o > 0$
Q_3,Q_4 Off			$V_s / 2$	$-V_s / 2$	V_s	D_4,D_2 if $i_o < 0$

The inverter output root-mean-square (rms) voltage value can be found as

$$V_o = \left(\frac{2}{T_0} \int_0^{T_0/2} V^2{}_S \, dt \right)^{1/2} = V_S \tag{1.1}$$

The inverter instantaneous output voltage can be found from the Fourier series as

$$v_o = \sum_{n=1,3,5,\ldots}^{\infty} \frac{4V_S}{n\pi} \sin(n\omega t) \tag{1.2}$$

1.3 Pulse Width Modulation (PWM)

Pulse width modulation is the most popular technique used in industrial drives such as inverters, rectifiers and DC choppers. The principle of this technique depends on comparing a carrier wave with a reference wave which always comes from the switching strategy for such control algorithm. This comparison generates the required gating signals to the power switches. Sinusoidal PWM is widely used to control H-bridge inverters due to the low harmonic distortion in the inverter output voltage waveform. Sinusoidal PWM (SPWM) can be categorized in three various types as bipolar, unipolar, and multicarrier PWM [5].

The advantages and disadvantages of the bipolar and unipolar SPWM will be discussed in the following sections, while multicarrier PWM will not be discussed here because it is used in multilevel converters which is not related to the thesis topic.

1.3.1 Bipolar Sinusoidal Pulse Width Modulation

In bipolar sinusoidal PWM, the reference signal V_{ref} is compared with the carrier signal (triangle wave) V_{cr}. For the case when $V_{ref} > V_{cr}$, the digital gating circuit generates an active high pulse (logic1) to control the power switches Q_1 and Q_2, then a positive voltage V_s will appear in the inverter output terminals (a, b). On the other hand; when $V_{ref} < V_{cr}$ the digital gating circuit generates an active high pulse to control the power switches Q_3 and Q_4, then a negative voltage $-V_s$ will appear in the inverter output terminals (a, b). As a result, the inverter output voltage contains two voltage levels V_s and $-V_s$ in the positive or negative half cycle [3]. Figure 1.4 illustrates the bipolar SPWM for single phase full bridge inverter.

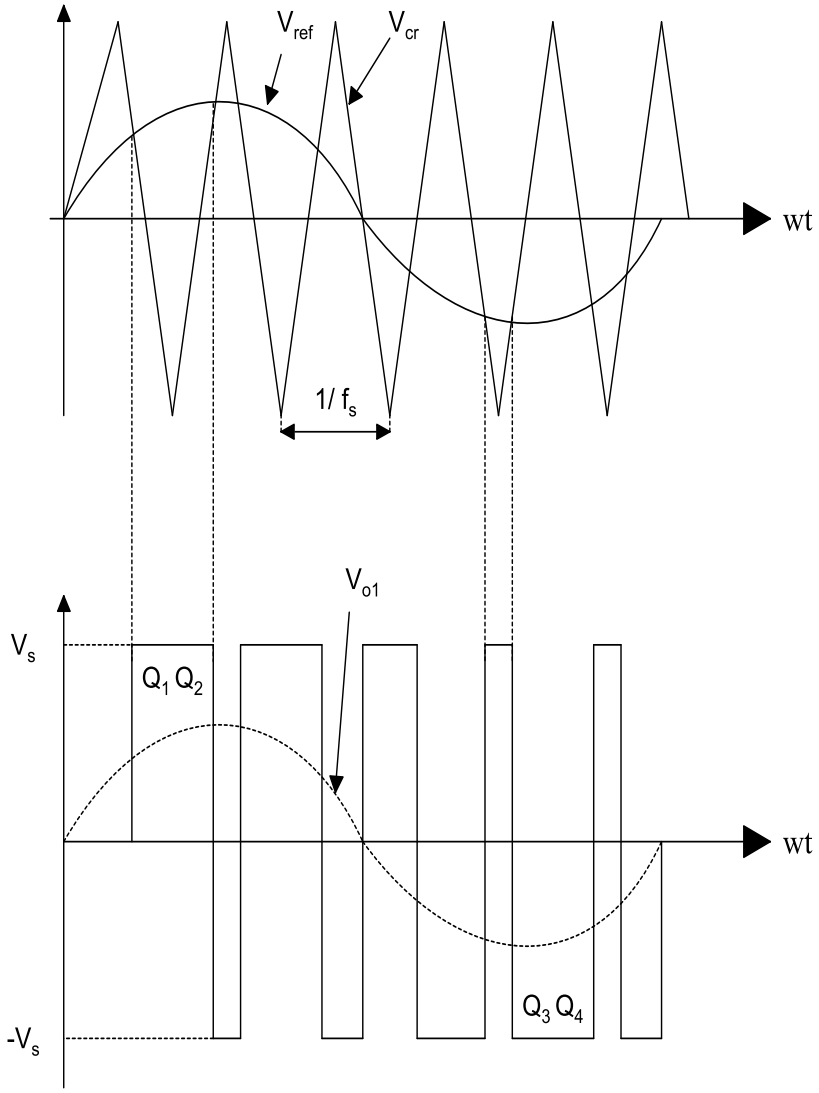

Figure 1.4: Bipolar SPWM for single phase full bridge inverter [4].

1.3.2 Unipolar Sinusoidal Pulse Width Modulation

Unipolar SPWM can be generated by employing two carrier signals shifted by 180 degrees and one reference signal [3], or by one carrier signal and two reference signals shifted by 180 degrees [4]. In fact, unipolar SPWM is a combination of two opposite bipolar SPWM, each one being responsible to generate the required gating signal for each H-bridge leg. Figure 1.5 illustrates the unipolar SPWM for single phase full bridge inverter.

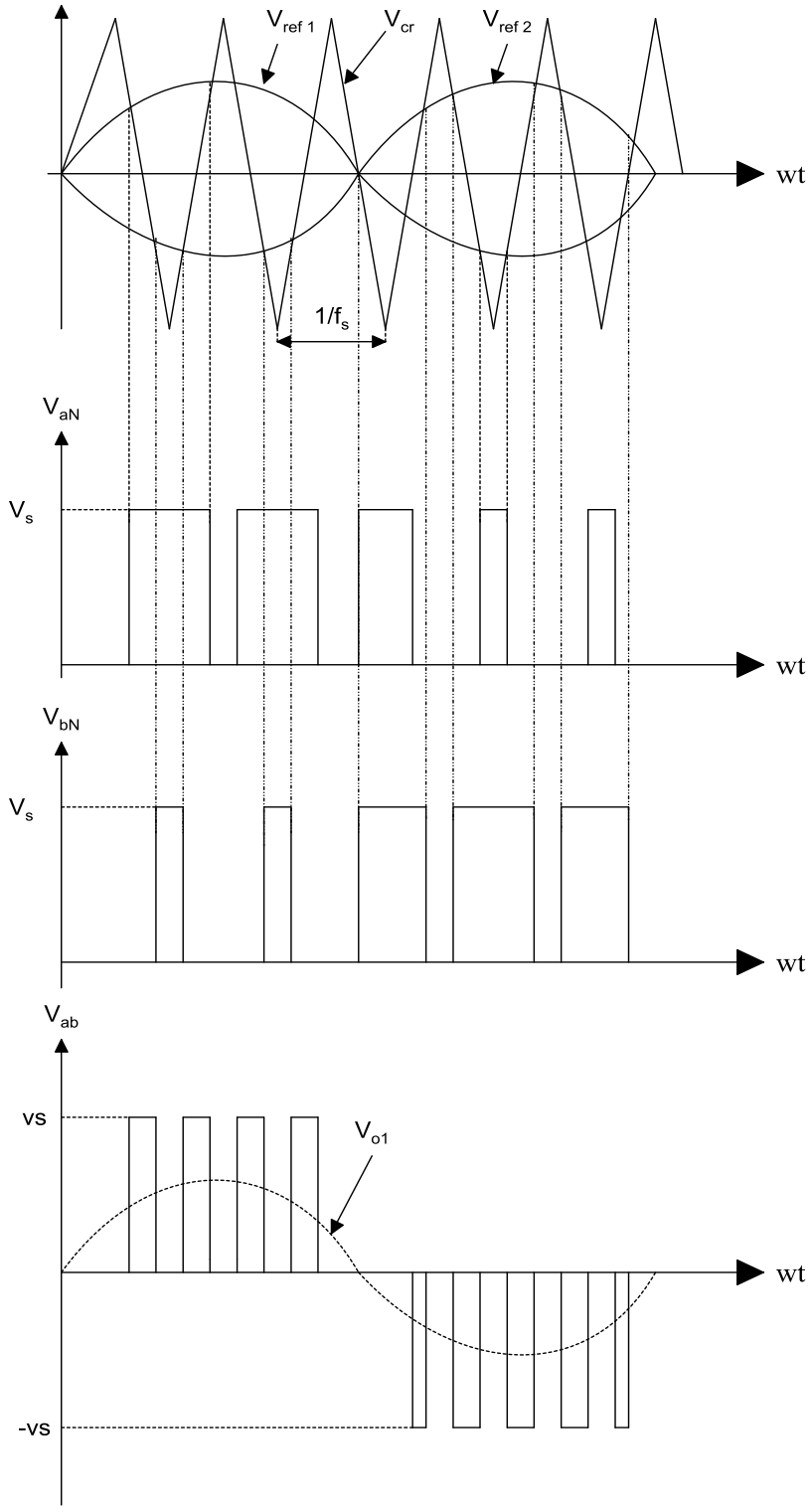

Figure 1.5: Unipolar SPWM for single phase full bridge inverter [4].

Notice that, the inverter output voltage contains three voltage levels V_s, zero and $-V_s$ in the positive or in the negative half cycle. Unipolar SPWM has several advantages over bipolar SPWM, which can be summarized as [5]:

- Output voltage has no even harmonic.
- Harmonic content is half of the bipolar type.
- The significant harmonics appear around twice the switching frequency.

1.4 Thesis Objective

The objective of this thesis is to investigate predictive strategies for the current control of grid-connected single-phase inverters. The control objectives are to obtain currents with as low total harmonic distortion (THD) as possible and to inject the power from the inverter with high power factor (ideally unity).

1.5 Thesis Organization

Thesis structure organize as follows; in chapter 1, we introduce the renewable energy advantages and we give briefly explanation for single phase inverter, in chapter 2 we give a short review of current control methods, in chapter 3 we mention the grid connected inverter operation modes then the predictive current controllers with its both type the traditional and improved control and the stability for each system is discussed, then in chapter 4 we include the simulation results for the proposed controllers, conclusions and future works recommendations are given in chapter 5.

Chapter 2

REVIEW OF CURRENT CONTROL METHODS

For the application of grid-connected inverters, the output voltage and frequency of the inverter should be equal to the grid voltage and frequency respectively. For renewable energy applications, a voltage source inverter is to be used with regulated output current. The controller should be able to regulate (control) its output current such that adequate performance is achieved.

There are many approaches that have been presented in the literature to come up with a proper controller which is capable of solving the problem of grid-connected inverters. Here, a general review of the basic approaches to handle the problem is discussed.

2.1 Hysteresis Controller

In the hysteresis control method, the line current is measured and compared with a reference current value within a boundary of error called hysteresis (h), shown in Figure 2.1. The hysteresis is the value of the maximum deviation allowed from the measured current to its corresponding reference, assuming there is no delay from the controller and the inverter [6]

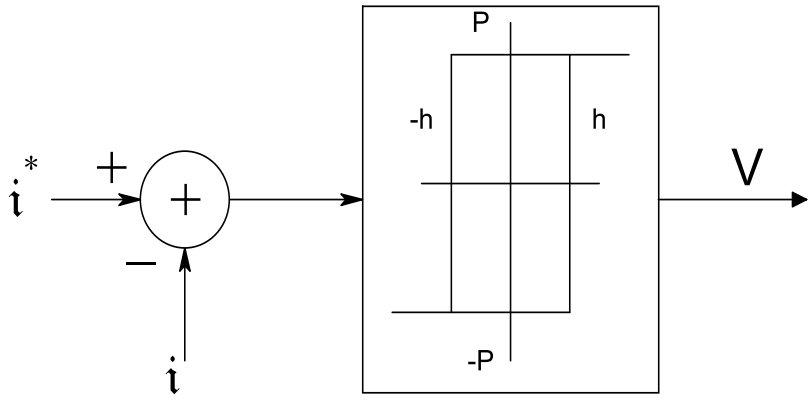

Figure 2.1: Hysteresis controller [6].

If the measured value of the line current is greater than its reference, the inverter switches such that –P is applied to the load side. If the opposite happens, the inverter switches are activated so +P is applied to the load, resulting in an instantaneous current limit if the neutral is connected to the dc bus. If there is no neutral connection, the current reaches double the hysteresis band [6].

Because the current ripple is specified around boundary value and the ripple is constant, the inverter switching frequency will be around that value or maybe multiple of that value. This gives the inverter a wide variable switching frequency. Therefore, the inverter should be capable of handling the maximum switching frequency that may occur.

This control method has two main disadvantages. First is the insensitivity to parameter variation, because the controller applies either –P or +P to the load side. The second is rapid convergence for large scale current error value.

2.1.1 Sinusoidal band hysteresis control

In this method, the value of lowest and the highest switching frequencies is spread out over large range of frequencies. This means that the low and the high possible

switching frequencies are away from each other, so there will be difficulty in designing a filter which can handle and treat this large range of frequencies. To solve this problem, the switching frequency can be fixed, so that a simple filter is used. A simple method is to adjust the bandwidth (H) to take the sinusoidal waveform. The lower and the higher band are in sinusoidal form [8].

This method has the advantages of reducing the harmonic content of the inverter output filter and fixed switching frequency operation, but it suffers from the complexity of requiring complex real-time calculations in the high frequency range and for variable grid-side voltage or the source side voltage. The complexity of the calculations means more processors are required to control (calculate) the value of H, which is not practical for the grid connected inverter applications.

2.1.2 Triangle Band Hysteresis

In this method, a simplified triangle hysteresis band is replaced by the sinusoidal one. Using the triangle form instead of the sinusoidal waveform will reduce the required microprocessor memory.

Here, only two points are to be calculated, low and high value of the boundary. As a result, for example in 50 Hz application, we need only four points in each cycle to be calculated and a linear line to be connected from a point to the next one, while in sinusoidal application the calculation of the boundary should be executed at each sampling period. This method has simplicity of implementation, fixed switching frequency with low total harmonic distortion (THD) value in addition to saving processor memory [8].

2.2 Some Methods to Maintain Variable Hysteresis Band

Basically, a hysteresis controller is based on the principle of comparing the required reference current with the measured current so that the switching state of the inverter is controlled. There are many approaches to achieve constant switching frequency for variable hysteresis band controller. Some of them are listed below.

2.2.1 From the current error and its derivative.

For the application in AC motors, forward and feedback control methods are used to accomplish variable hysteresis band and then compensate for the interaction between phase back emfs that occur when the neutral of a three phase motor is left floating [9].

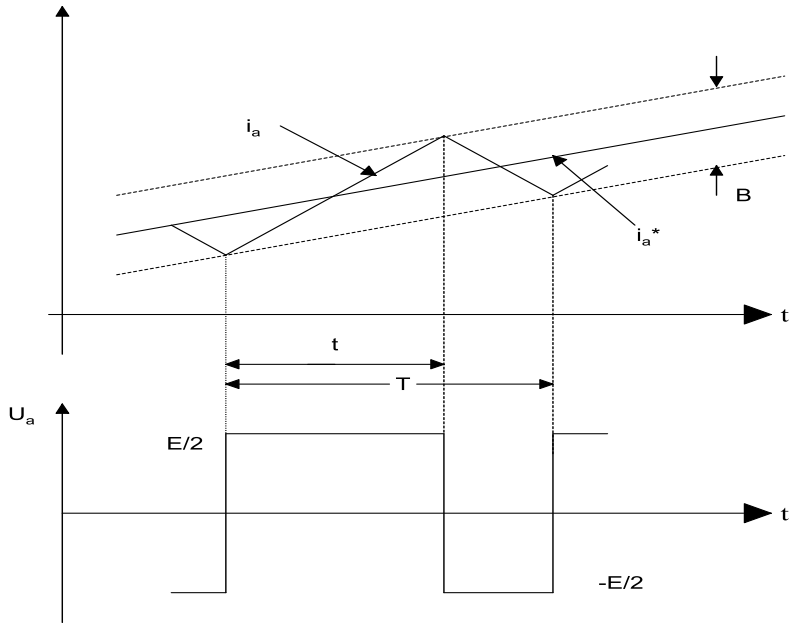

Figure 2.2: Hysteresis band current controller [9].

This controller has low steady state error, high performance with good dynamic response. This controller is independent of load variations.

2.2.2 From current error zero crossings

Calculating the required hysteresis band variation that synchronizes the current error zero-crossings to an external clock results in constant switching frequency. While this method has good performance, it still suffers from the computation complexity; the processor should be capable of handling the instant calculation each duration.

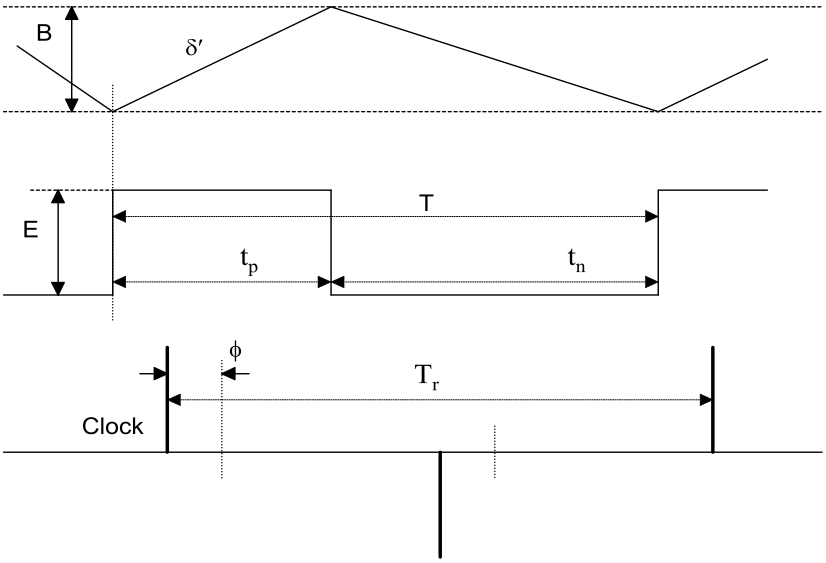

Figure 2.3: Hysteresis comparator operation [10].

In three-phase applications, three individual current regulators are required to be installed, one for each phase leg. This will reduce the controller efficiency because of the phase-to-leg interaction problem [10].

2.2.3 From the average voltages

Calculating the inverter average output voltage of the phase-leg is an approximation of the back emfs in AC applications. This average is to be used to vary the hysteresis band such that a constant switching frequency is maintained. There are many other modifications added to this method to refine the controller by fine tuning the hysteresis band [11], [12]. By comparing the current error zero-crossing with fixed reference clock, fine-tuned control of the switching frequency is maintained.

The result of the proposed method gives a fixed output switching frequency. Furthermore, the proposed strategy is extended for only two phase-leg controller such that hysteresis current regulation is achieved. The third leg is switched using normal PWM with reference voltage as an average of the other two switched legs (which are already switched).

2.3 Ramp Comparison Controller

Figure 2.2 shows a ramp comparison controller. This type of controller is established on the methodology of comparing the modulated current error signal to an actual current signal. The comparison logic is designed such that if the modulated current error signal is greater than the value of the current signal, then the inverter will be switched on, and if the modulated current error is greater than the current signal the inverter signal will switch off.

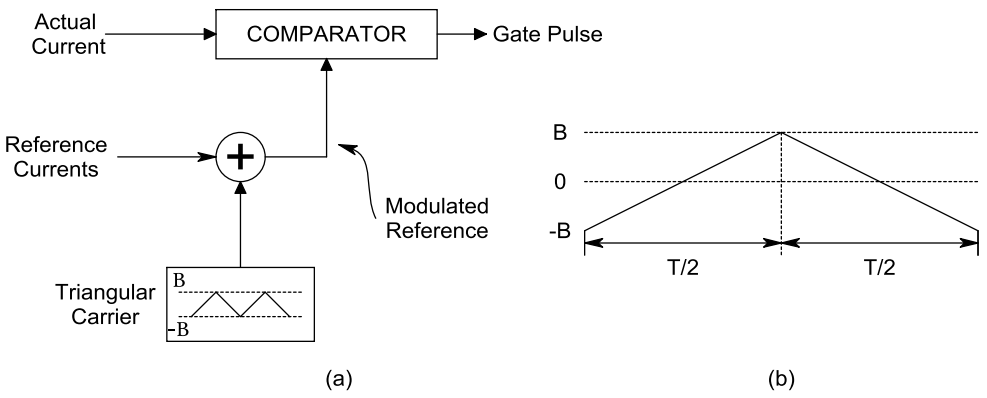

Figure 2.4: (a) Ramp comparison controller. (b) One period of carrier [7].

By applying this strategy, the inverter switching frequency will be equal to the triangle waveform reference and the harmonics produced from the switching strategy will be specific and known in advance.

At high switching speed and when the error rate of change is greater than the rate of change of the sinusoidal reference, the error value of the controller will increase and there will be steady state error. This means that, the overall efficiency of the controller is reduced. To overcome this problem, the controller gain should be adjusted by modifying the amplitude of the reference signal or by applying integral compensation to the current error signal [7].

This method suffers from the problem of over-crossing, which occurs when the slope of the actual current is greater than the slope of the modulated reference current. To solve this problem, a condition should be applied to the comparator such that the maximum slope magnitude of the actual current must be less than the minimum slope magnitude of the modulated reference current signal [13].

2.4 Single Band Current Controller

In [14], a very simple and robust method of current control is presented. The control signals of the grid connected inverter are derived directly from the voltage grid, and applied to the control switches. Firstly, the grid voltage is to be measured, and then the current reference value is to be derived from the measured grid voltage as

$$\frac{d\delta}{dt} = \frac{V_{dc} - V_g}{L_f} \tag{2.1}$$

Such that δ represents the output current error (i.e. $i_o = i_r + \delta$).

This method will ensure unity power factor for the power injected to the grid. That is because the current reference used is in phase with the grid voltage. It is already derived from the grid voltage. Figure 2.3 shows the main construction of the proposed controller.

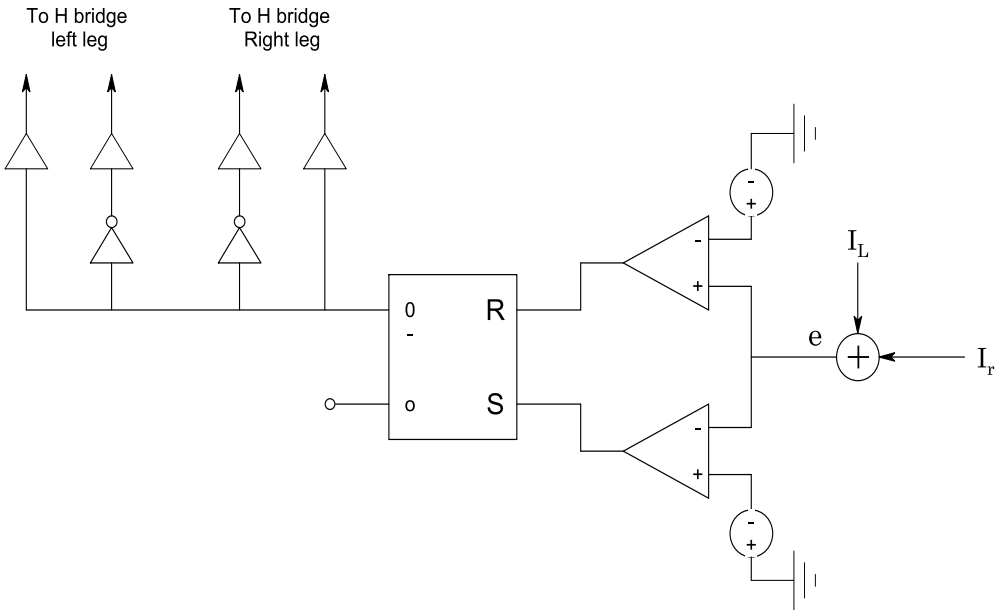

Figure 2.5: The proposed controller construction [14].

The authors of [14] have derived an equation for switching frequency estimation given by

$$f_s = \frac{V_{dc}(1-k^2\sin^2(wt))}{4L_f h} \tag{2.2}$$

such that *k* represents the modulation index $\frac{V_m}{V_{dc}}$. The grid reference voltage is given by $V_g = V_m \sin wt$. The proposed control method has average switching frequency given by

$$f_{s,av} = \frac{V_{dc}}{4L_f h}(1-\frac{k^2}{2}) \tag{2.3}$$

with maximum switching frequency up to $\frac{V_{dc}}{4L_f h}$.

The inverter has single-band hysteresis current control with two level output voltage with no zero level output voltage. When this method is used, there is no need for a compensator or phase locked loop (PLL). It has simplicity and robustness compared

to conventional control methods. Nevertheless, this method has high switching frequency and difficulty of implementation when higher current values are to be injected to the grid.

Chapter 3

PREDICTIVE CURRENT CONTROL STRATEGIES

Predictive current control (PCC) approach is based on calculating the required inverter output voltage such that the actual current follows the reference current. Nowadays, the availability of fast and low cost digital signal processer boards (DSP's) makes the implementation of predictive controllers simpler and sufficient.

3.1 Traditional PCC for Single Phase Voltage Source Grid inverter

3.1.1 Traditional PCC algorithm

Figure 3.1 shows the general structure of a single-phase H-bridge grid-connected inverter. The inverter operates in four different modes. Two modes operate in the positive half-cycle and the other two operate in the negative half-cycle. Table 3.1 illustrates the different operating modes [15].

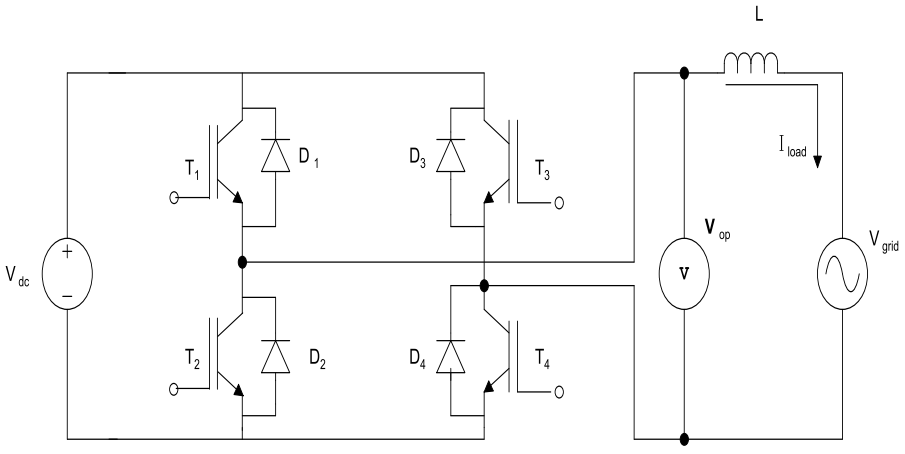

Figure 3.1: Single Phase H- Bridge Grid Connected Inverter [15].

Table 3.1: Switching states of Single phase full bridge grid inverter [15].

Mode	T_1	T_2	T_3	T_4	D_3	D_4	V_{op}	I_{load}
1	ON	OFF	OFF	ON	OFF	OFF	V_{dc}	Pos
2	ON	OFF	OFF	OFF	ON	OFF	0	Pos
3	OFF	ON	ON	OFF	OFF	OFF	$-V_{dc}$	Neg
4	OFF	ON	OFF	OFF	OFF	ON	0	Neg

Referring to Figure 3.1, the mathematical form of the required inverter output voltage can be written as the following differential equation:

$$V_{op} = V_{grid} + L\frac{di_{load}}{dt} \tag{3.1}$$

Where V_{op} is the inverter terminal output voltage, V_{grid} is the grid voltage and L is the series filter inductance with negligible internal resistance.

Assuming that the system operates with fixed switching frequency, the grid voltage and the load current are known (measured); a simple and direct predictive current control algorithm is proposed in [16] and [15]. With constant switching interval T_{period} (3.1) can be written in discrete-time form as

$$V_{op-av}[n] = V_{grid-av}[n] + L\frac{I_{load}[n+1] - I_{load}[n]}{T_{period}} \tag{3.2}$$

where $V_{op-av}[n]$ is the average required inverter output voltage during the switching interval $[n, n+1]$, $V_{grid-av}[n]$ is the average grid voltage during the switching interval $[n, n+1]$, T_{period} is the constant switching period, $I_{load}[n]$ and $I_{load}[n+1]$ are the measured currents at the sampling points $[n]$ and $[n+1]$, respectively.

The predictive current controller's (PCC) goal is to force $I_{load}[n+1]$ to be equal the reference current $I_{ref}[n+1]$ at the sampling point $[n+1]$ so that, $I_{load}[n+1]$ can be replaced with $I_{ref}[n+1]$ and equation (3.2) can be written as

$$V_{op-av}[n] = V_{grid-av}[n] + L\frac{I_{ref}[n+1] - I_{load}[n]}{T_{period}} \tag{3.3}$$

In real implementation, the controller needs a certain time to do the required digital sampling and computations before the control command proceeds to the inverter switches. This means that, the digital controller cannot solve for $V_{op-av}[n]$ because $V_{grid-av}[n]$ and $I_{load}[n]$ are not available for the controller in the switching interval $[n, n+1]$. To solve these obstacles, a certain adjustment to the control equation (3.3) is required.

In [16] D.Holmes and D.Martin suggested using the previous switching period results in order to estimate a proper average grid voltage and load current values. Figure 3.2 shows the traditional PC controller timing schematic for the proposed algorithm.

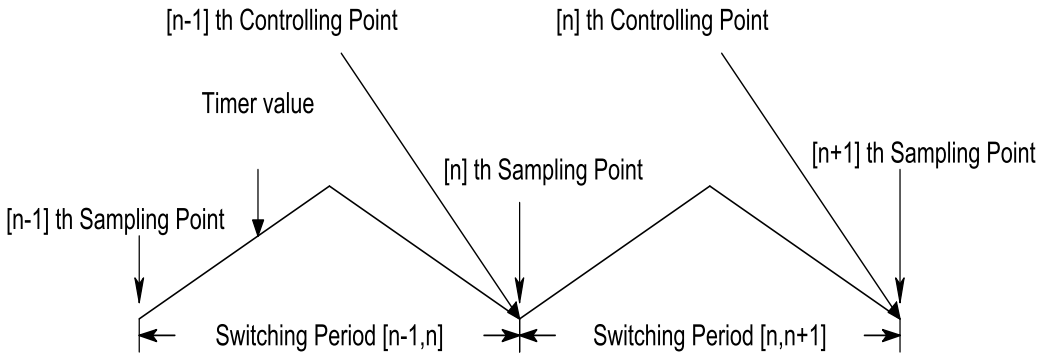

Figure 3.2: Traditional PCC Timing Diagram [4].

Referring to Figure 3.2, it is obvious that the controller should use the measured values of the load current $I_{load}[n-1]$ and grid voltage $V_{grid}[n-1]$ which are available when the calculations start at the beginning of switching interval $[n-1, n]$. Then, the required average inverter output voltage will be applied in the interval $[n, n+1]$. This average inverter voltage can be used in any proper pulse width modulation (PWM) circuit to generate the required inverter gating signals. Figure 3.3 shows the traditional predictive current control system block diagram.

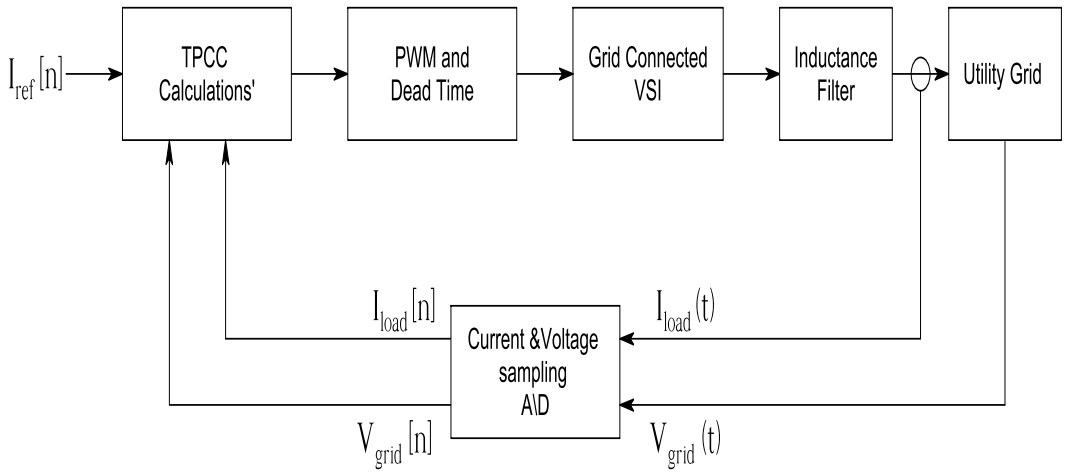

Figure 3.3: Traditional PCC system block diagram.

3.1.2 Average Grid Voltage Linear Extrapolation Estimation

With the known previous grid voltage average value, the average grid voltage over the switching interval $[n, n+1]$ can be estimated by using the simple linear extrapolation [16], [17]. Figure 3.4 illustrates the switching intervals with the average grid voltage values.

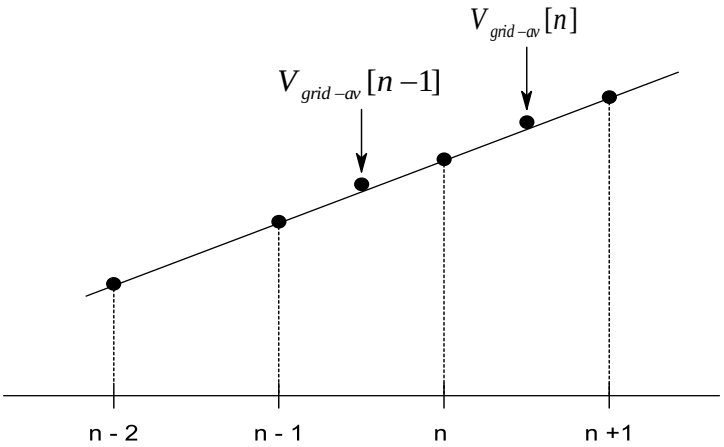

Figure 3.4: Switching intervals with the average grid voltage values.

In Figure 3.4, we assume that the grid voltage change during the intervals is linear and this change is equal from one interval to the other. Then the average grid voltage over the interval $[n, n+1]$ can be written as :

$$V_{grid-av}[n] = \frac{V_{grid}[n+1] + V_{grid}[n]}{2} \tag{3.4}$$

The grid voltage value at the sampling point $[n+1]$ can be predicted as

$$V_{grid}[n+1] = V_{grid}[n] + \Delta V_{grid} \tag{3.5}$$

Where ΔV_{grid} is the grid voltage change during the switching interval, since the inverter operates with fixed switching frequency we can assume that ΔV_{grid} is constant in any interval.

Taking the interval $[n-1, n]$, then ΔV_{grid} can be written as

$$\Delta V_{grid} = V_{grid}[n] - V_{grid}[n-1] \tag{3.6}$$

substituting equation (3.6) into equation (3.5) lead to

$$V_{grid}[n+1] = V_{grid}[n] + (V_{grid}[n] - V_{grid}[n-1]) \tag{3.7}$$

Then for the interval $[n-2, n-1]$, $V_{grid}[n]$ can be written as :

$$V_{grid}[n]=V_{grid}[n-1]+(V_{grid}[n-1]-V_{grid}[n-2]) \tag{3.8}$$

Substituting equation (3.7) and equation (3.8) into equation (3.4) leads to

$$V_{grid-av}[n]=\frac{5}{2}V_{grid}[n-1]-\frac{3}{2}V_{grid}[n-2] \tag{3.9}$$

Notice that $V_{grid-av}[n]$ can be calculated by substituting equation (3.7) into (3.4). We have

$$V_{grid-av}[n]=\frac{3}{2}V_{grid}[n]-\frac{1}{2}V_{grid}[n-1] \tag{3.10}$$

3.1.3 Load Current Estimation

Under the same assumption that the inverter operates with constant switching frequency and linear voltage change, we can assume that the load current is linearly changed with the inverter voltage change.

We can rewrite (3.2) for the sampling point $[n-1]$ as

$$V_{op-av}[n-1]=V_{grid-av}[n-1]+L\frac{I_{load}[n]-I_{load}[n-1]}{T_{period}} \tag{3.11}$$

Solving equation (3.11) for $I_{load}[n]$ lead to

$$I_{load}[n]=I_{load}[n-1]+\frac{T_{period}}{L}\left(V_{op-av}[n-1]-V_{grid-av}[n-1]\right) \tag{3.12}$$

We can rewrite (3.10) for the sampling point $[n-1]$ as

$$V_{grid-av}[n-1]=\frac{3}{2}V_{grid}[n-1]-\frac{1}{2}V_{grid}[n-2] \tag{3.13}$$

Substituting equation (3.13) into (3.12) leads to

$$I_{load}[n]=I_{load}[n-1]+\frac{T_{period}}{L}\left(V_{op-av}[n-1]-\frac{3V_{grid}[n-1]-V_{grid}[n-2]}{2}\right) \tag{3.14}$$

From (3.14), it is clear that the load current at time $[n]$ is estimated by adding the mustered load current $I_{load}[n-1]$ at point $[n-1]$ to the predicted current change in the switching interval $[n-1,n]$. Figure 3.5 illustrates the switching intervals with the load current values.

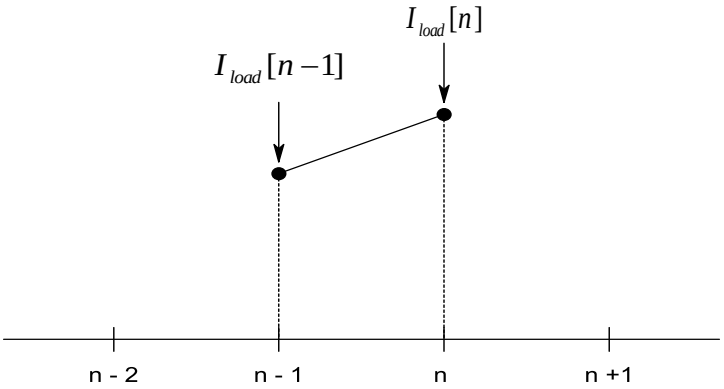

Figure 3.5: Switching intervals with the load current values.

3.1.4 Traditional Predictive Current Control Equation

The estimated average grid voltage and load currant given by (3.9) and (3.14), respectively, can be substituted in (3.3) to give the traditional predictive current control (TPCC) equation as

$$V_{op-av}[n] = 4V_{grid}[n-1] - 2V_{grid}[n-2] - V_{0\,p-av}[n-1] + L\frac{I_{ref}[n+1] - I_{load}[n-1]}{T_{period}} \quad (3.15)$$

From (3.15) we notice that, all values are available to the controller when the calculation proceeds at time point $[n-1]$ and the result will be applied during the switching interval $[n, n+1]$.

3.2 Improved Predictive Current Control for Single Phase Grid Inverter

In TPCC, the controller starts the calculation at the beginning of the previous switching interval and the result will be applied to the next interval. This means, the

controller has full switching interval time to do the algorithm computations. Low switching frequencies are used for high power applications. So as a result, with the availability of high speed controllers we can conclude that this given time is more than enough and it can be reduced further more.

An improved predictive current control algorithm is developed by setting the sampling point just ahead the controlling point by the total sampling and computation delay (T_D). Figure 3.6 shows the improved predictive current control (IPCC) timing schematic for the proposed algorithm.

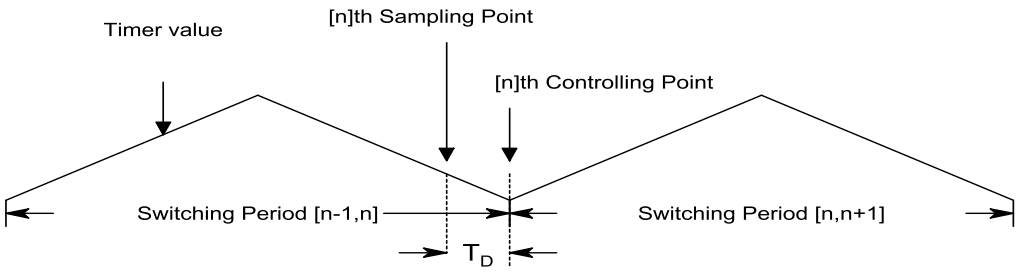

Figure 3.6: Improved PCC timing diagram [8].

As mentioned in Figure 3.6, the sampling point is set at time $[nT_{period} - T_D]$. T_D is very small compared to T_{period}, with fast controllers and low switching frequencies for power applications, we can assume that this delay time is negligible.

With the above assumption, we can write the load current $I_{load}[n]$ and the grid voltage $V_{grid}[n]$ as

$$I_{load}[n] \cong I_{load}[nT_{period} - T_D] \tag{3.16}$$

$$V_{grid}[n] \cong V_{grid}[nT_{period} - T_D] \tag{3.17}$$

From above, the values of $I_{load}[n]$ and $V_{grid}[n]$ are available to the controller at time $[nT_{period} - T_D]$ so the calculations can proceed and the result will be applied in the switching interval $[n, n+1]$.

By substituting (3.10) into (3.3) the control equation for IPCC can be written as

$$V_{op-av}[n] = \frac{3}{2}V_{grid}[n] - \frac{1}{2}V_{grid}[n-1] + L\,\frac{I_{ref}[n+1] - I_{load}[n]}{T_{period}} \qquad (3.18)$$

Comparing (3.18) to (3.15) it is clear that the improved algorithm has simple computation process and gives more enhanced performance for the injected power to the grid. The details will be discussed in section (3.5) and will be verified using Matlab simulation, while results are to be presented in Chapter 4.

3.3 Linear Sine Wave Prediction

3.3.1 Average Grid Voltage Linear Sine Wave Prediction

In previous TPCC and IPCC the controller uses the linear extrapolation approach for grid voltage prediction. But actually, we have sinusoidal grid voltage waveform. This means that if we use the linear sine wave prediction (LSWP) instead of linear extrapolation prediction, the control algorithm gives more accurate result in the current phase shift.

From [18] the linear sine wave grid voltage prediction equation can be written as

$$V_{grid}[n] = 2\cos\omega_s\, V_{grid}[n-1] - V_{grid}[n-2] \qquad (3.19)$$

where ω_s is the discrete-time sampling frequency.

The grid voltage prediction for the sampling point $[n+1]$ is given as

$$V_{grid}[n+1] = 2\cos\omega_s\, V_{grid}[n] - V_{grid}[n-1] \qquad (3.20)$$

Substituting equation (3.19) into equation (3.20) gives:

$$V_{grid}[n+1]=(4\cos^2\omega_s-1)V_{grid}[n-1]-(2\cos\omega_s)V_{grid}[n-2] \tag{3.21}$$

The average grid voltage prediction can be written as :

$$V_{grid-av}[n]=\frac{V_{grid}[n]+V_{grid}[n+1]}{2} \tag{3.22}$$

Substituting equation (3.19) and (3.21) into equation (3.22) lead to:

$$V_{grid-av}[n]=(\cos\omega_s+2\cos^2\omega_s-\frac{1}{2})V_{grid}[n-1]-(\frac{1}{2}+\cos\omega_s)V_{grid}[n-2] \tag{3.23}$$

3.3.2 Load Current Estimation

The load current at time $[n]$ can be estimated by adding the mustered load current $I_{load}[n-1]$ at point $[n-1]$ to the predicted current change in the switching interval $[n-1,n]$. The predicted load current at time $[n]$ can be written as:

$$I_{load}[n]=I_{load}[n-1]+\frac{T_{period}}{L}\left[V_{op-av}[n-1]-\left((\cos\omega_s+2\cos^2\omega_s-\frac{1}{2})V_{grid}[n-2]-(\frac{1}{2}+\cos\omega_s)V_{grid}[n-3]\right)\right] \tag{3.24}$$

3.4 Controller Equations with Linear Sine wave Grid Voltage prediction

3.4.1 Traditional Predictive Current Control Equation With LSWP

Traditional controller uses the previous switching intervals to control the inverter power switches. Now we want to apply the linear sine wave prediction which is illustrated in Section 3.3. To obtain the TPCC control equation, this can be easily done by substituting (3.24) into (3.3) as

$$\begin{aligned}V_{op-av}[n]=V_{grid-av}[n]+\frac{L}{T_{period}}(I_{ref}[n+1]-I_{load}[n-1])-V_{op-av}[n-1]\\+(\cos\omega_s+2\cos^2\omega_s-\frac{1}{2})V_{grid}[n-2]-(\frac{1}{2}+\cos\omega_s)V_{grid}[n-3]\end{aligned} \tag{3.25}$$

where $V_{grid-av}[n]$ is the predicted grid voltage given in (3.23).

3.4.2 Improved Predictive Current Control Equation With LSWP

In improved control, the values of $I_{load}[n]$ and $V_{grid}[n]$ are available to the controller at time $[nT_{period} - T_D]$ so the calculations can proceed and the result will be applied in the switching interval $[n, n+1]$. The average grid voltage with LSWP at time instant $[n]$ can be written as

$$V_{grid-av}[n] = (\frac{1}{2} + \cos\omega_s)V_{grid}[n] - \frac{1}{2}V_{grid}[n-1] \quad (3.26)$$

The improved current control equation with LSWP can be written as :

$$V_{op-av}[n] = (\frac{1}{2} + \cos\omega_s)V_{grid}[n] - \frac{1}{2}V_{grid}[n-1] + \frac{L}{T_{period}}(I_{ref}[n+1] - I_{load}[n]) \quad (3.27)$$

Again improved algorithm has simple computation process and gives more enhanced performance for the power injected to the grid. The details will be discussed in Chapter 4.

3.5 PWM Implementation

The PWM process depends on comparing a triangle wave (carrier) to a reference wave. For the discrete-time algorithm the comparison occurs in each switching period independently. Figure 3.7 illustrates the PWM for single-phase inverter.

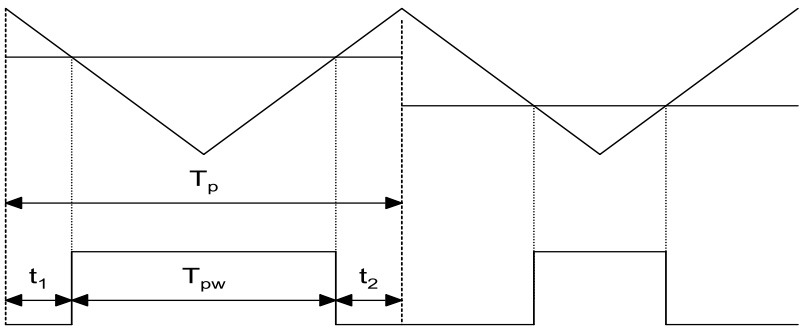

Figure 3.7: PWM for single-phase inverter.

The pulse width T_{pw} can be calculated as

$$T_{pw} = \frac{V_{op-av}[n]}{V_{dc}} T_p \tag{3.28}$$

The active low pulse $t_1 = t_2$ is calculated as

$$t_1 = \frac{T_p}{2}\left(1 - \frac{V_{op-av}[n]}{V_{dc}}\right) \tag{3.29}$$

3.6 Stability Analysis

In the previous sections, four different approaches were introduced. Two for traditional control and another two for improved control. The stability for traditional and improved algorithms is established from the closed loop pole locations which should be inside the unit circle such that the system is stable.

From the controller equations, we notice that the average inverter voltage depends on the filter inductance value. Any variation in this value (due to the heating effect, saturation or disturbance) will affect the stability of the system.

3.6.1 Close Loop System for TPCC

From equations (3.14) and (3.15) the load current $I_{load}[n], I_{load}[n-1]$ and the average inverter voltage $V_{op-av}[n-1]$ are set as state variables. The close loop system equations are given in Appendix A. The state equations are given by

$$\begin{bmatrix} I_{load}[n] \\ I_{load}[n+1] \\ V_{op-av}[n] \end{bmatrix} = \begin{bmatrix} 0 & 1 & 0 \\ -\frac{Lm}{L} & 1 & -\frac{T_p}{L} \\ -\frac{Lm}{T_p} & 0 & -1 \end{bmatrix} \begin{bmatrix} I_{load}[n-1] \\ I_{load}[n] \\ V_{op-av}[n-1] \end{bmatrix} + \begin{bmatrix} 0 & 0 & 0 & 0 \\ \frac{L_m}{L} & \frac{4T_p}{L} & -\frac{2T_p}{L} & -\frac{T_p}{L} \\ \frac{L_m}{T_p} & 4 & -2 & 0 \end{bmatrix} \begin{bmatrix} I_{ref}[n+1] \\ V_{grid}[n-1] \\ V_{grid}[n-2] \\ V_{grid-av}[n] \end{bmatrix} \tag{3.30}$$

where L_m is the modeled inductance value.

The characteristic equation of the TPCC closed loop system is

$$Z^3 + (\frac{L_m}{L} - 1)Z = 0 \tag{3.31}$$

The TPCC closed loop poles are

$$P_1 = 0 \ , P_{2,3} = \pm\sqrt{\Delta_L}$$

where $\Delta_L = \frac{L - L_m}{L}$ is the relative error between the actual filter inductance and the modeled filter inductance.

The relative inductance error Δ_L has positive value when the actual inductance is greater than the modeled inductance. One pole will be set on the positive half of the real axis of the unit circle and the other one will be set on the negative half real axis of the unit circle and the third pole is located at the origin. The relative inductance error Δ_L has negative value when the actual inductance is less than the modeled inductance. So one pole will be set on the positive half of the imaginary axis of the

unit circle and the other one will be set on the negative half of the imaginary axis of the unit circle and the third pole is located at the origin. Figure 3.8 illustrates the TPCC close loop pole locations in the unit circle.

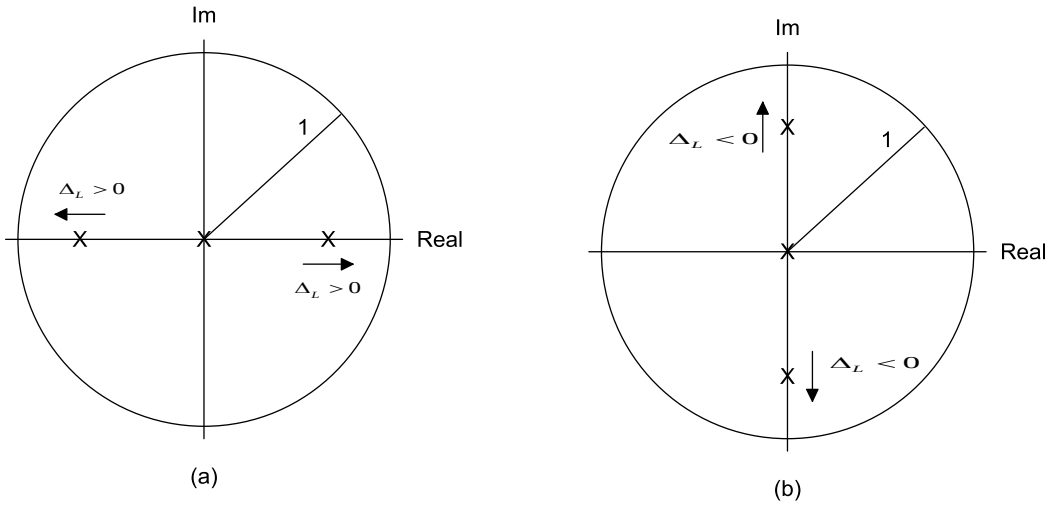

Figure 3.8: TPCC close loop poles locations (a) with positive Δ_L (b) with negative Δ_L .

Refer to Figure 3.7 the stable range of the relative inductance error is

$$-1 \le \Delta_L \le 1$$

Then the TPCC modeled inductance stable range is

$$0 \le L_m \le 2L$$

3.6.2 Close loop System for IPCC

The load current $I_{load}[n]$ and the average inverter voltage $V_{op-av}[n-1]$ are set as state variables. The closed loop system is derived in Appendix B as

$$\begin{bmatrix} I_{load}[n+1] \\ V_{op-av}[n] \end{bmatrix} = \begin{bmatrix} \Delta_L & 0 \\ -\dfrac{Lm}{T_p} & 0 \end{bmatrix} \begin{bmatrix} I_{load}[n] \\ V_{op-av}[n-1] \end{bmatrix} + \begin{bmatrix} 0 & 0 & 1-\Delta_L \\ -\dfrac{1}{2} & \dfrac{3}{2} & \dfrac{Lm}{T_p} \end{bmatrix} \begin{bmatrix} V_{grid}[n-1] \\ V_{grid}[n] \\ I_{ref}[n+1] \end{bmatrix} \quad (3.32)$$

The characteristic equation of the IPCC closed loop system is

$$Z(Z-\Delta_L)=0 \quad (3.33)$$

The IPCC closed loop poles are:

$$P_1 = 0 \ , P_2 = \Delta_L$$

The relative inductance error Δ_L has positive value when the actual inductance is greater than the modeled inductance. One pole will be set on the positive half of the real axis of the unit circle and other one will be set at the origin. The relative inductance error Δ_L has negative value when the actual inductance is less than the modeled inductance. So one pole will be set on the negative half of the real axis of the unit circle and the other one will be set at the origin. Figure 3.9 illustrate the IPCC closed loop pole locations.

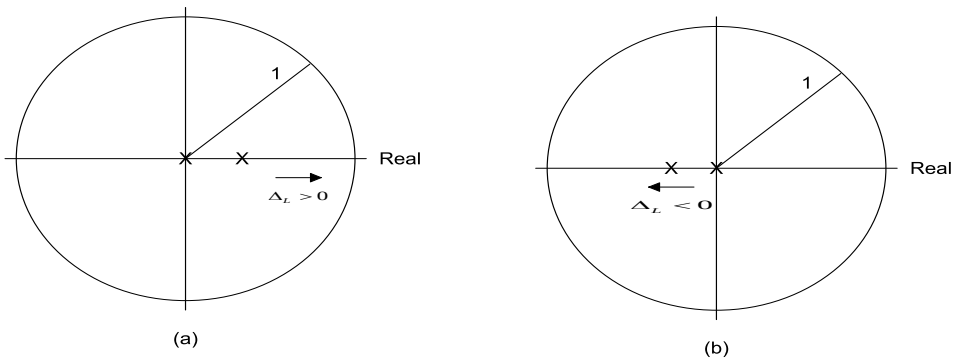

Figure 3.9: IPCC close loop poles locations (a) with positive Δ_L ; (b) with negative Δ_L .

Refer to Figure 3.9, the stable range of the relative inductance error is :

$$-1 \leq \Delta_L \leq 1$$

Then the IPCC modeled inductance stable range is :

$$0 \leq L_m \leq 2L$$

Notice that the TPCC and IPCC algorithms have the same stable range under system parameter variation, but for certain filter inductance error Δ_L the IPCC poles will be nearest to the origin, which implies more stability (robustness) of the IPCC algorithm.

Chapter 4

SIMULATION RESULTS

4.1 Introduction

In this chapter we introduce the computer simulation results for the single-phase grid connected inverter with the proposed predictive current controllers.

The parameters of the single-phase grid-connected inverter simulated in Matlab-Simulink are given in Table 4.1.

Table 4.1: Grid-connected inverter parameters.

Grid Line-to Neutral Voltage	240 Vrms
Grid Frequency	60Hz
DC Link Voltage	400 V
Rated Power	10 Kw
Filter Inductance	2mH
Switching Frequency	10 kHz

4.2 TPCC With Linear Extrapolation Grid Voltage Prediction

The TPCC illustrated in Section 3.1.4 is simulated using Matlab code given in Appendix C. The inverter output voltage and current are shown in Figure 4.1

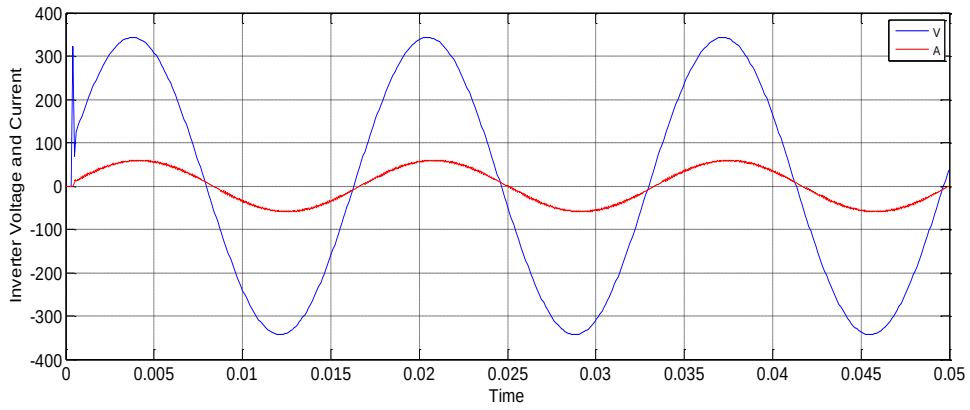

(a)

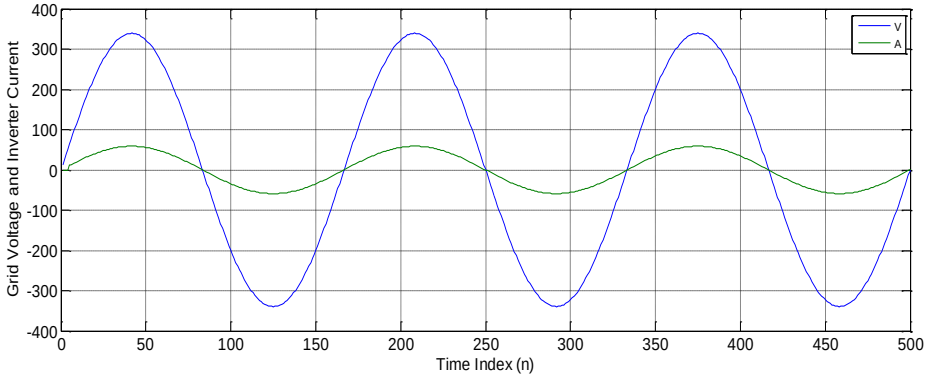

(b)

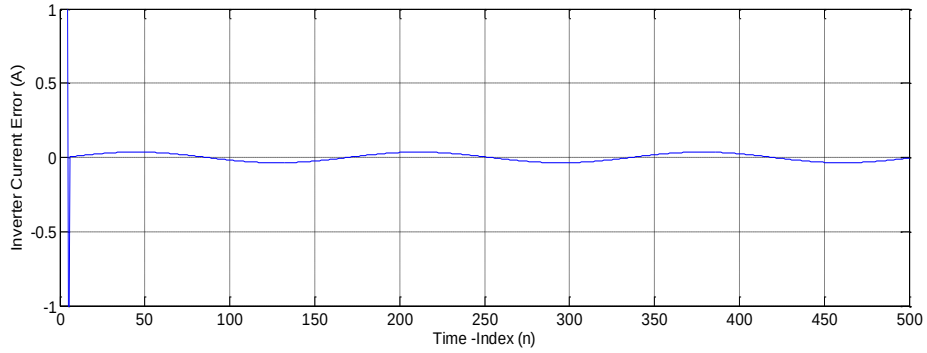

(c)

Figure 4.1: TPCC with linear extrapolation prediction Simulation wave forms (a) Inverter output voltage and current. (b) Grid voltage and inverter current. (c) Inverter current error.

4.3 IPCC With Linear Extrapolation Grid Voltage Prediction

The IPCC illustrated in section 3.2 is simulated using Matlab code given in appendix C. The inverter output voltage and current are shown in Figure 4.2.

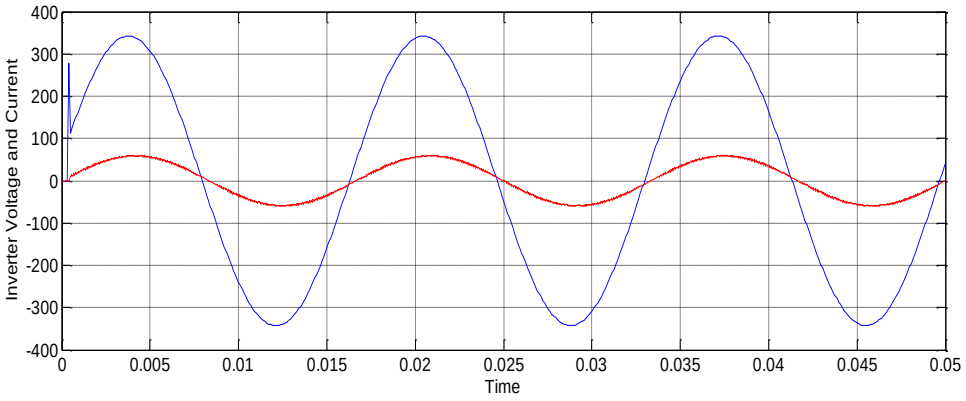

(a)

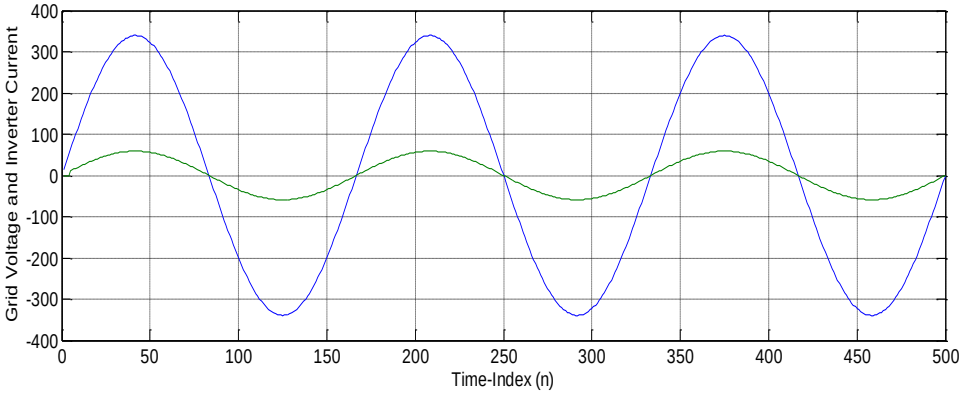

(b)

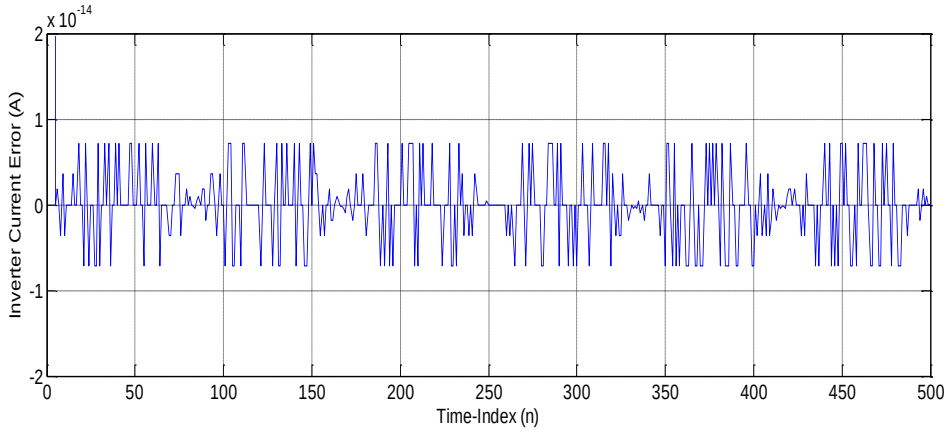

(c)

Figure 4.2: IPCC with linear extrapolation prediction simulation waveforms (a) inverter output voltage and current (b) grid voltage and inverter current. (c) inverter current error.

4.4 Inductance variation for TPCC and IPCC with Linear Extrapolation Grid Voltage Prediction.

For positive relative inductance error ($\Delta_L > 0$) the IPCC and TPCC approaches are simulated with three different modeled filter inductance values ($Lm = 0.9L$, $Lm = 0.6L$, $Lm = 0.2L$). The inverter output voltage waveforms with TPCC and IPCC are shown in Figure 4.3 and Figure 4.4 respectively.

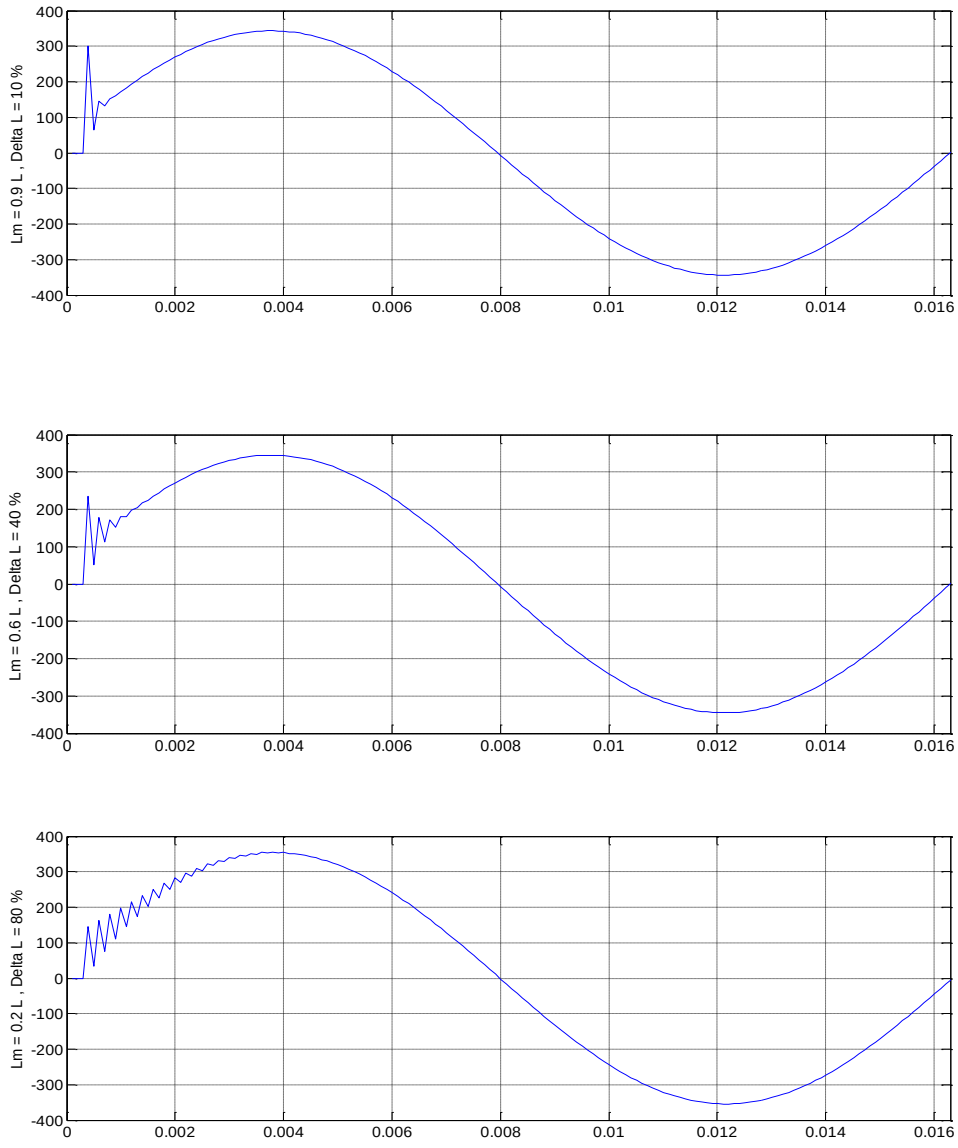

Figure 4.3: Model mismatch effect ($\Delta_L > 0$) on the inverter output voltage waveforms for TPCC with linear extrapolation prediction.

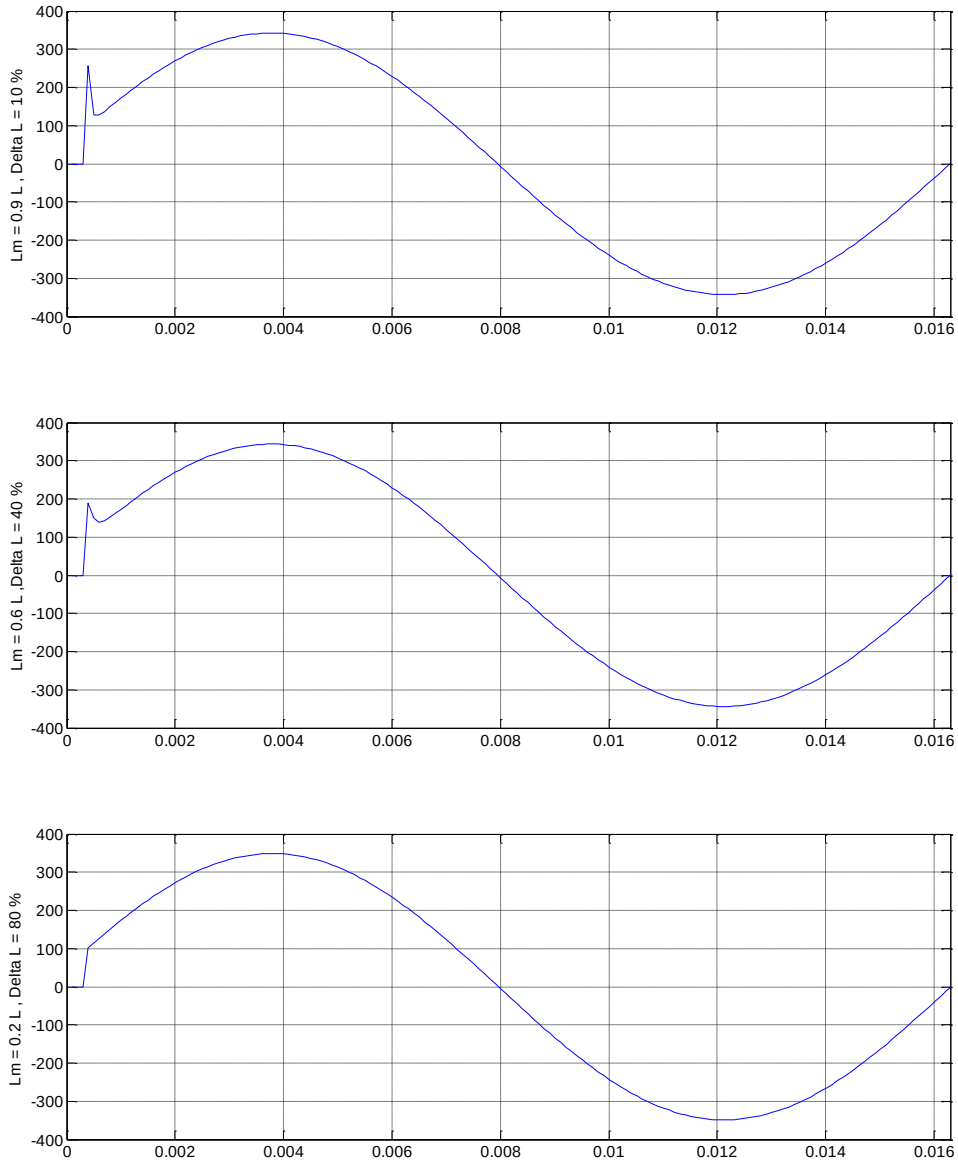

Figure 4.4: Model mismatch effect ($\Delta_L > 0$) on the inverter output voltage waveforms for IPCC with linear extrapolation prediction.

Referring to Figure 4.1 and Figure 4.2 we can notice that the IPCC has lowest current error than TPCC. Current error values are shown in Table 4.2 and the current error plots are shown in Figure 4.5. Comparing Figure 4.3 and Figure 4.4 the TPCC inverter output voltage starts to oscillate when $\Delta_L = 40\%$, while the IPCC has almost no oscillation (robust), so the conclusion drawn in Section 3.6 is verified.

Table 4.2: Peak inverter current error at 10KHz switching frequency , L = 2 mH .

Lm	Current Error for TPCC with LEXP	Current Error for IPCC with LEXP	Current Error for TPCC with LSWP	Current Error for IPCC with LSWP
0.7 L	1.89	0.95	1.9	0.95
0.8 L	1.1	0.55	1.1	0.55
0.9 L	0.49	0.24	0.49	0.24
L	0.036	$1.9*10^{-14}$	$3*10^{-4}$	$1.6*10^{-14}$
1.3 L	1.027	0.51	1.02	0.51
1.6 L	1.66	0.83	1.66	0.83
1.9 L	2.1	1.052	2.1	1.052
2 L	4.37	2.57	4.3	1.27

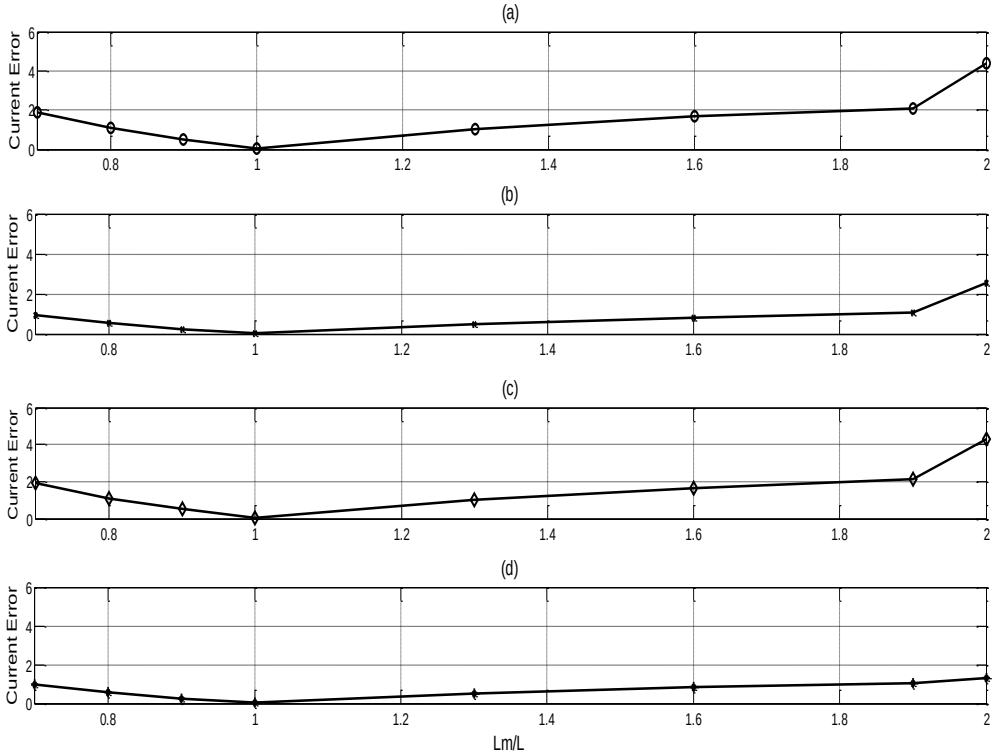

Figure 4.5: Peak inverter current error values with inductance model mismatching. (a)for TPCC with linear extrapolation prediction. (b) for IPCC with linear extrapolation prediction. (c) for TPCC with linear sine wave prediction. (d) for IPCC with linear sine wave prediction.

For negative relative inductance error ($\Delta_L < 0$) The IPCC and TPCC approaches are simulated with three different modeled filter inductance values ($L_m = 1.3L$, $L_m = 1.6L$, $L_m = 1.8L$). The inverter output voltage waveforms with TPCC and IPCC are shown in Figure 4.6 and Figure 4.7 respectively. Notice that again the IPCC maintained more robustness. The closed loop system poles are shown in Figure 4.8.

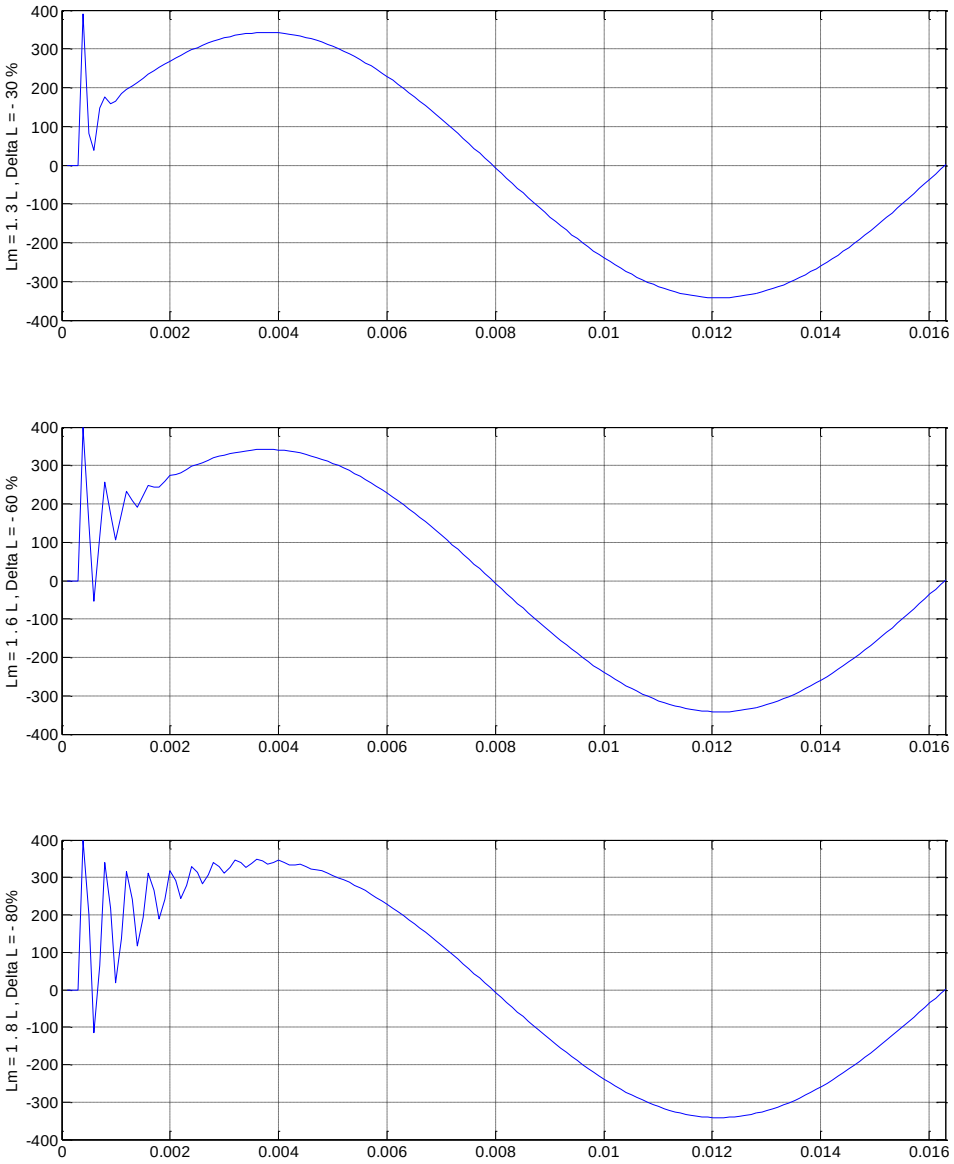

Figure 4.6: Model mismatch effect ($\Delta_L < 0$) on the inverter output voltage waveforms for TPCC with linear extrapolation prediction.

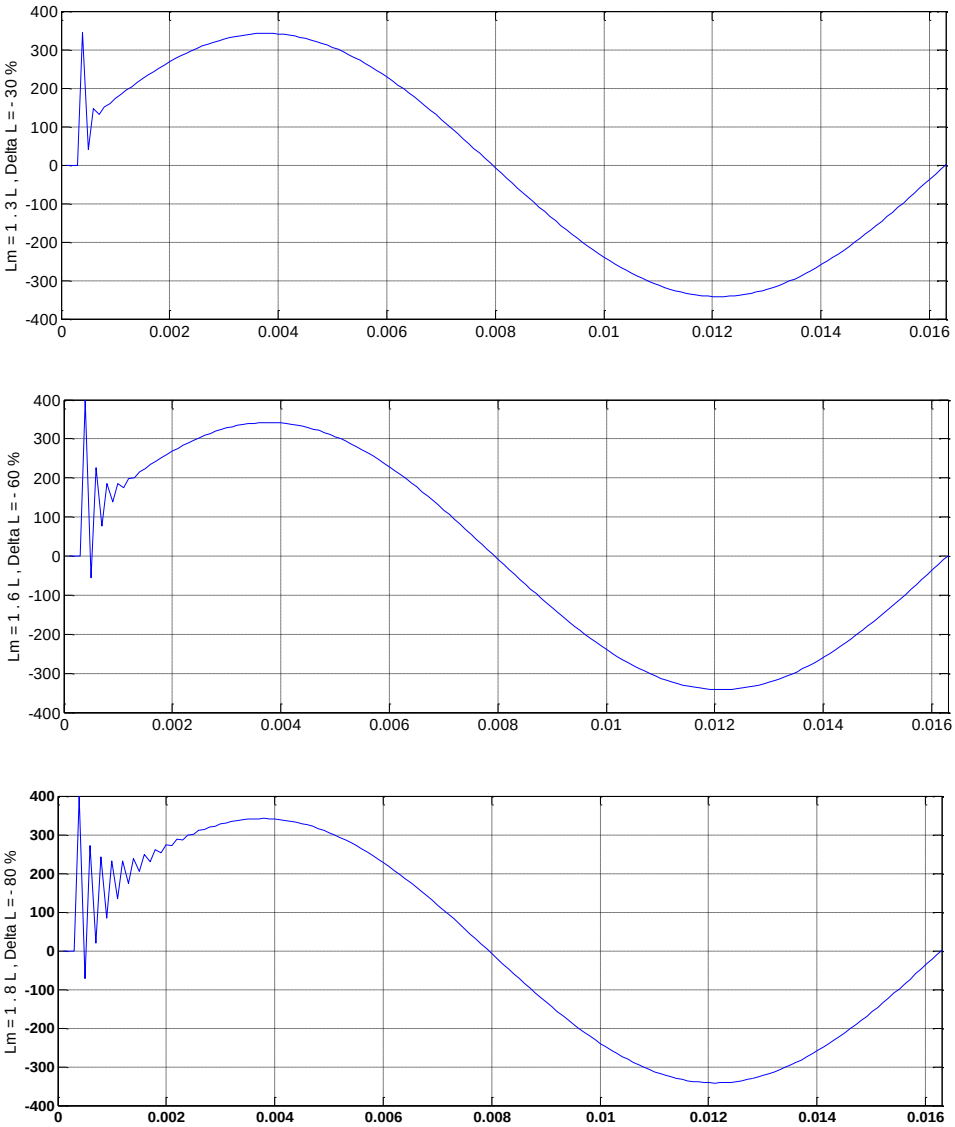

Figure 4.7: Model mismatch effect ($\Delta_L < 0$) on the inverter output voltage waveforms for IPCC with linear extrapolation prediction.

The inverter current THD for different filter inductance variations with 10 kHz and 2.5 kHz switching frequencies are shown in Table 4.3 and Table 4.4 respectively. Moreover, The THD values during the filter inductance variation for all controllers at 10 kHz and 2.5 kHz are shown in Figure 4.9 and in Figure 4.10 respectively.

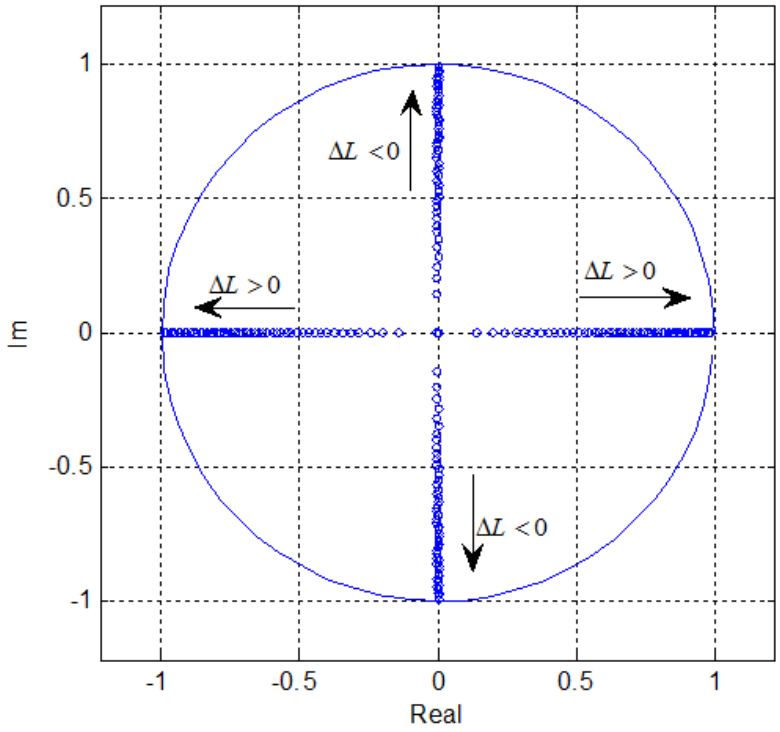

(a)

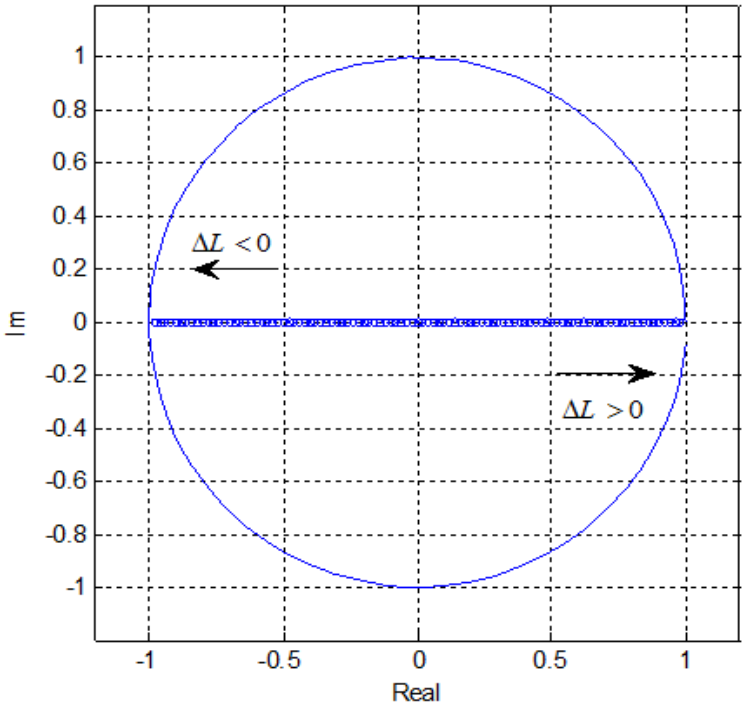

(b)

Figure 4.8: Closed loop poles plot for $0 \le L_m \le 2L$,0.00004 step size (a) TPCC poles. (b) IPCC poles.

Table 4.3: Inverter current THD at 10 KHz switching frequency, L = 2 mH .

Lm	Current THD% for TPCC with LEXP	Current THD% for IPCC with LEXP	Current THD% for TPCC with LSWP	Current THD% for IPCC with LSWP
0.7 L	2.6802	2.6849	2.6850	2.6867
0.8 L	2.6819	2.6866	2.6870	2.6884
0.9 L	2.6838	2.6880	2.6891	2.6898
L	2.6856	2.6892	2.6910	2.6910
1.3 L	2.6901	2.6920	2.6959	2.6937
1.6 L	2.6936	2.6938	2.6996	2.6956
1.9 L	2.6962	2.6952	2.7024	2.6969
2 L	4.0787	3.1853	4.1199	3.1909

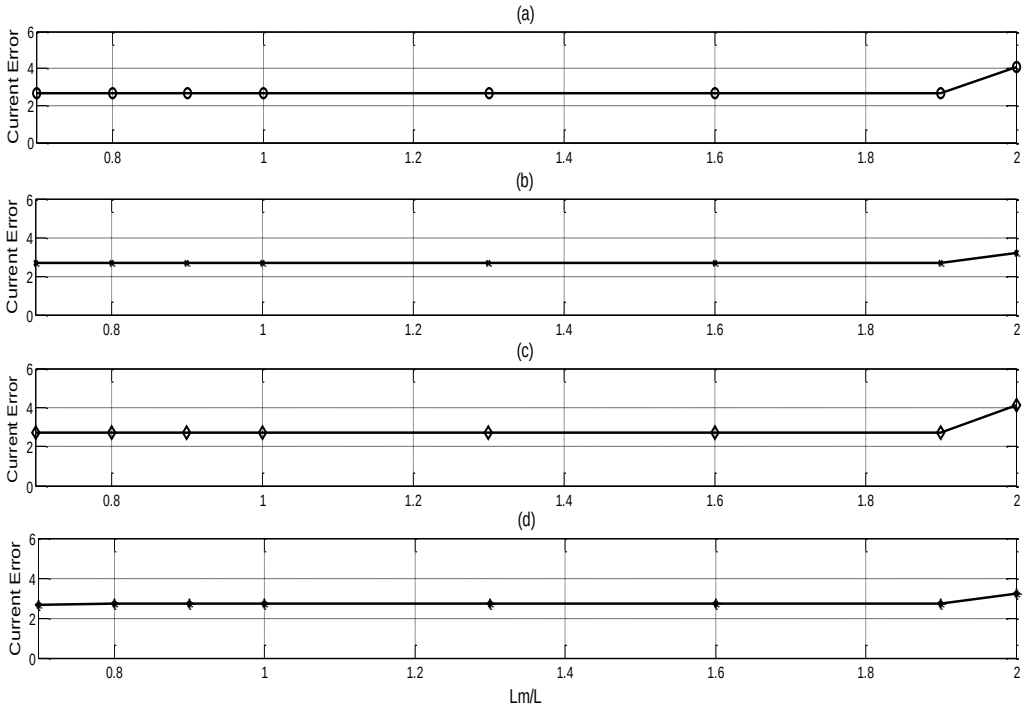

Figure 4.9: Inverter current THD % values with inductance model mismatching at10kHz switching frequency. (a) for TPCC with linear extrapolation prediction. (b)for IPCC with linear extrapolation prediction. (c) for TPCC with linear sine wave prediction. (d) for IPCC with linear sine wave prediction.

Table 4.4: Inverter current THD at 2.5 KHz switching frequency, L = 6 mH .

Lm	Current THD% For TPCC With LEXP	Current THD% For IPCC With LEXP	Current THD% For TPCC With LSWP	Current THD% For IPCC With LSWP
0.7 L	3.5292	3.5356	3.5902	3.5729
L	3.5371	3.5883	3.6239	3.6239
1.3 L	3.5916	3.6258	3.6806	3.6600
2 L	4.9384	3.9218	5.3176	4.2156

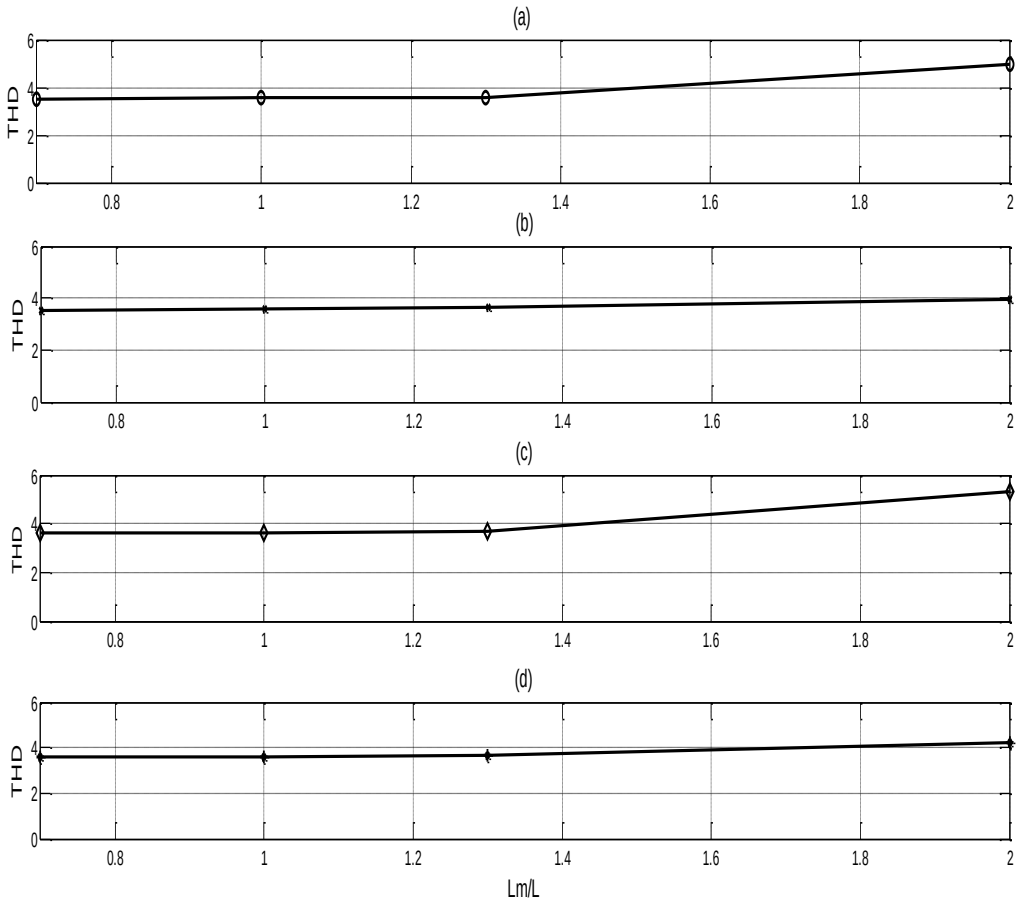

Figure 4.10: Inverter current THD % values with inductance model mismatching at 2.5 kHz switching frequency. (a) for TPCC with linear extrapolation prediction. (b) for IPCC with linear extrapolation prediction. (c) for TPCC with linear sine wave prediction. (d) for IPCC with linear sine wave prediction.

4.5 TPCC with Linear Sine Wave Grid Voltage Prediction

The TPCC illustrated in section 3.4.1 is simulated using Matlab code given in Appendix C. The inverter output voltage and current are shown in Figure 4.11.

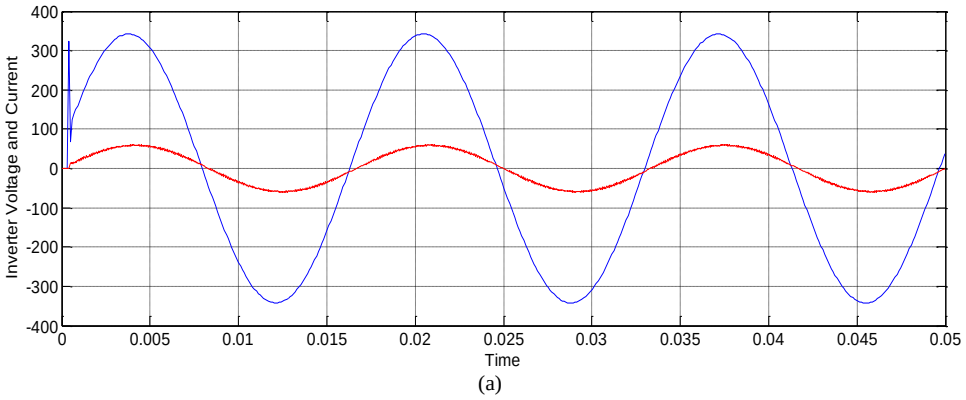

(a)

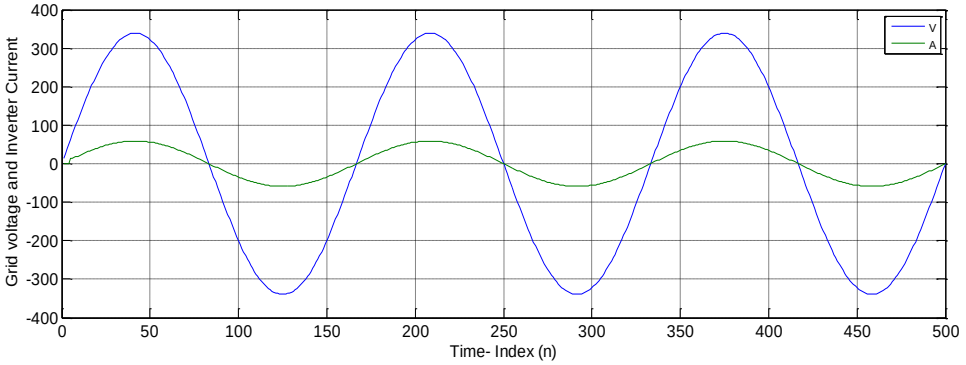

(b)

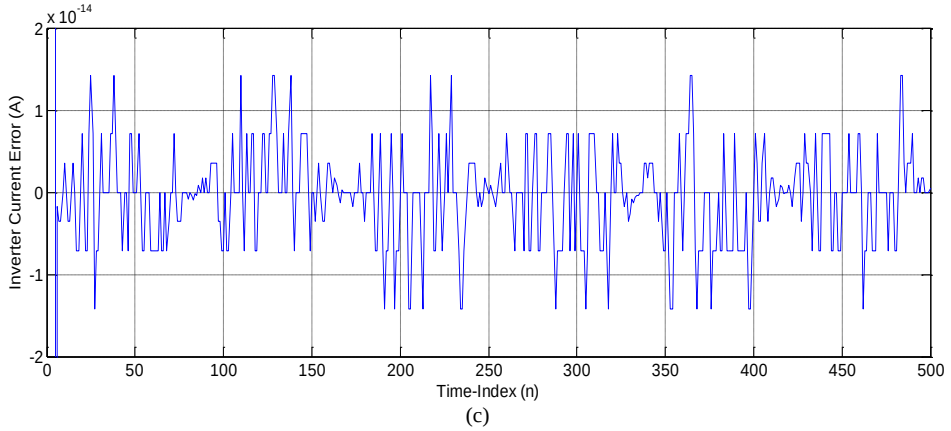

(c)

Figure 4.11: TPCC with LSWP Simulation wave forms (a) inverter output voltage and current.(b) grid voltage and inverter current. (c) inverter current error.

4.6 IPCC with Linear Sine Wave Grid Voltage Prediction

The IPCC illustrated in section 3.4.2 is simulated using Matlab code given in Appendix C. The inverter output voltage and current are shown in Figure 4.12.

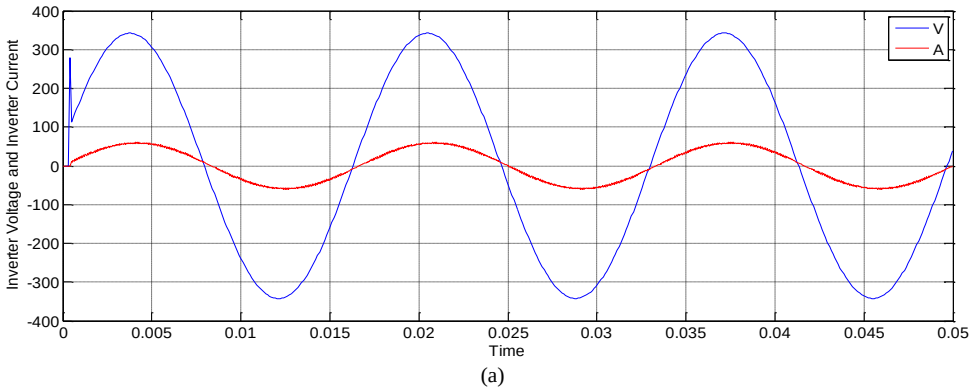

(a)

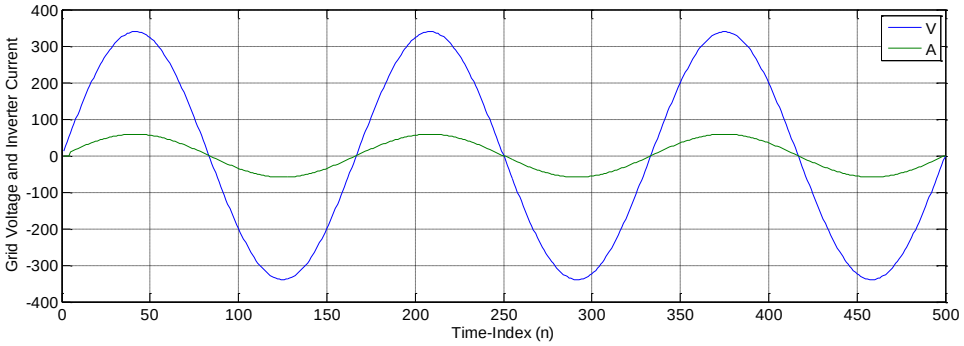

(b)

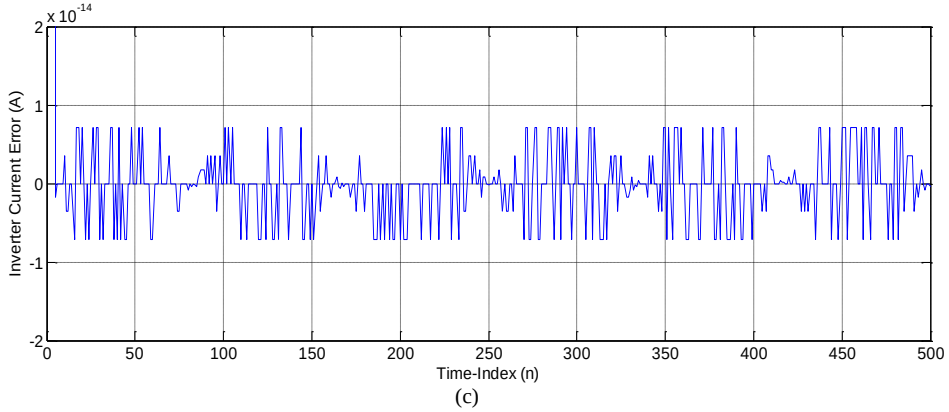

(c)

Figure 4.12: IPCC with LSWP Simulation wave forms (a) inverter output voltage and current.(b) grid voltage and inverter current. (c) inverter current error.

The predictive current control with linear sine wave grid voltage prediction achieve low phase shift angle between the injected current and the grid voltage especially in

low switching frequencies. This gives better performance for the power injected to the utility grid. The inverter current phase angles are displayed in Table 4.5 and plots in Figure 4.13.

Table 4.5: Inverter current angle (deg.) at 1.5KHz switching frequency, L= 2 mH.

Lm	Current Angle For TPCC With LEXP	Current Angle For IPCC With LEXP	Current Angle For TPCC With LSWP	Current Angle For IPCC With LSWP
0.7 L	0.6105	-6.5431	-0.5673	-6.5663
0.8 L	3.2682	-4.0725	-3.1246	-4.0451
0.9 L	5.5828	-2.1222	-3.5922	-2.1446
L	7.5766	-0.5469	-0.5689	-0.5689
1.3 L	12.0583	2.7575	5.9605	2.7361
1.6 L	15.0376	4.8374	10.1599	4.8164
1.9 L	16.1900	6.2652	13.1283	6.2436
2 L	16.4924	6.9706	14.6718	6.7680

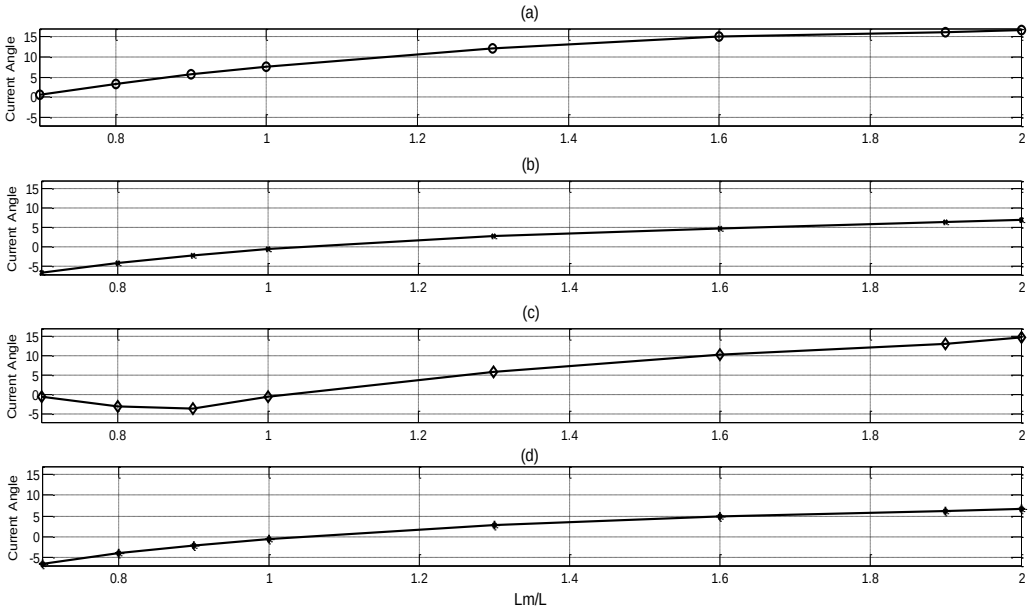

Figure 4.13: Inverter current angles (degree) with inductance model mismatching at 1.5 kHz switching frequency. (a) for TPCC with linear extrapolation prediction. (b) for IPCC with linear extrapolation prediction. (c) for TPCC with linear sine wave prediction. (d) for IPCC with linear sine wave prediction.

Chapter 5

CONCLUSION AND FUTURE WORK

5.1 Conclusion

In this thesis, the predictive current control method is employed to control a single-phase grid-connected inverter under the condition of measured grid voltage and load current. Both traditional and improved predictive current control approaches have acceptable THD according to IEEE standards, but the improved control has lowest steady state error. Traditional and improved predictive current control have the same stability range under filter inductance variation but the improved control has more robustness than the traditional control. Comparing the THD for traditional and improved control, the improved control has lowest THD in the critical upper stability range. The linear sine wave grid voltage prediction has better current phase angle than the linear extrapolation grid voltage prediction. This means, for traditional and improved control the LSWP is capable to give enhanced performance for the power injected especially in low switching frequencies range.

5.2 Future Work

For future work, an adaptive algorithm can be used to update the actual inductance value in the control equations. This updating may can give more enhancement to the inverter performance.

Also we recommend to use other type of filter such as L-C or L-C-L. This type of filters may ensure low distortion in the output voltage and current, so high performance can be added to the system.

REFERENCES

[1] M. H. Rashid, *Power Electronics Handbook*, Academic Press, 2001.

[2] B. K. Bose, *Modern Power Electronics and AC Drives*, Prentice Hall, Upper Saddle River, 2002.

[3] B. M. Wilamowski & J. D. Irwin, *The Industrial Electronics Handbook Power Electronic and Motor Drives*, 2nd ed., CRC Press: Taylor & Francis, 2011.

[4] Timothy L. Skvarenina, *The Power Electronics Handbook Industrial Electronics Series*, 2nd ed. CRC Press, 2002.

[5] A. Abrishamifar, A. Ahmad, & M. Mohamadian, "Fixed switching frequency sliding mode control for single-phase unipolar inverters," *IEEE Transactions on Power Electronics*, vol. 27, no. 5, pp. 2507-2517, 2012.

[6] Sepe, R. B., "A unified approach to hysteretic and ramp-comparison current controllers," *IEEE Annual Meeting of Industry Applications Society*, pp. 724-731, October 1993.

[7] Brod, David M., Donald W. Novotny, "Current control of VSI-PWM inverters," *IEEE Transactions Industry Applications*, vol 3, pp. 62-570, 1985.

[8] Zhang, Jie, et al. "Simplified variable band hysteresis current control for grid-connected inverter," *IEEE International Conference in Electrical Machines and Systems,* China, pp. 1-4, August 2011.

[9] Yao, Qunying, and D. G. Holmes. "A simple novel method for variable-hysteresis-band current control of a three phase inverter with constant switching frequency," *IEEE Annual Meeting of Industry Applications Society*, pp. 1122-1129, October 1993.

[10] Malesani, Luigi, Paolo Mattavelli, & Paolo Tomasin, "Improved constant-frequency hysteresis current control of VSI inverters with simple feed forward bandwidth prediction," *IEEE Transactions on Industry Applications*, vol. 33, no. 5, pp.1194-1202, 1997.

[11] Holmes, Reza Davoodnezhad, & Brendan P. McGrath, "An improved three-phase variable-band hysteresis current regulator," *IEEE Conference on Power Electronics*, Korea, pp. 961-978, June 2013.

[12] Holmes, Donald Grahame, Reza Davoodnezhad, & Brendan P. McGrath, "An improved three-phase variable-band hysteresis current regulator." *IEEE Transactions on Power Electronics*, vol. 28, on.1, pp. 441-450, 2013.

[13] Srikanthan, S., & Mahesh K. Mishra, "Constant frequency current control using a ramp comparison method for a DSTATCOM application." *IEEE Region 10 Conference,* India, no. 10, pp. 1-6, 2008.

[14] Rahim, N. A., & Jeyraj Selvara, "Implementation of hysteresis current control for single-phase grid connected inverter," *IEEE International Conference on Power Electronics and Drive Systems*, Malaysia, no. 7, pp. 1097-1101, 2007.

[15] Kojabadi, Hossein Madadi, Bin Yu, Idris A. Gadoura, Liuchen Chang, & Mohsen Ghribi, "A novel DSP-based current-controlled PWM strategy for single phase grid connected inverters." *IEEE Transactions on Power Electronics*,vol *21, no.4* pp. 985-993, July 2006.

[16] D. G. Holmes and D. A Martin, "Implementation of a direct digital predictive current controller for single and three phase voltage source inverter," *IEEE Annul Meeting on Industry Applications*, vol. 2, San Diego, pp. 906–913, 1996.

[17] Bode, Gerwich H., Poh Chiang Loh, Michael John Newman, & Donald Grahame Holmes, "An improved robust predictive current regulation algorithm," *IEEE Transactions on Industry Applications*, vol. 41, no. 6, pp. 1720-1733, December 2005.

[18] Maurice G. Bellanger, *Adaptive Digital Filters, Second Edition*, Marcel Dekker, 2001.

APPENDICES

Appendix A: Derivation of Equation (3.30)

The actual average inverter output voltage is:

$$V_{op-av}[n] = V_{grid-av}[n] + L\frac{I_{load}[n+1] - I_{load}[n]}{T_{period}} \tag{1A}$$

The controller calculate the average inverter output voltage as

$$V_{op-av}[n] = 4V_{grid}[n-1] - 2V_{grid}[n-2] - V_{0p-av}[n-1] + Lm\frac{I_{ref}[n+1] - I_{load}[n-1]}{T_{period}} \tag{2A}$$

The actual inverter current at time $[n+1]$ given as:

$$I_{load}[n+1] = I_{load}[n] + \frac{T_{period}}{L}\left(V_{op-av}[n] - V_{grid-av}[n]\right) \tag{3A}$$

Substitute (2A) in (3A) give:

$$\begin{aligned} I_{load}[n+1] = I_{load}[n] - \frac{Lm}{L} I_{load}[n-1] + \frac{Lm}{L} I_{ref}[n+1] \\ + \frac{T_{period}}{L}\left(4V_{grid}[n-1] - 2V_{grid}[n-2] - V_{0p-av}[n-1] - V_{grid-av}[n]\right) \end{aligned} \tag{4A}$$

The state variables are:

$$\begin{aligned} x_1[n] &= I_{load}[n-1] \\ x_2[n] &= I_{load}[n] \\ x_3[n] &= V_{op-av}(n-1) \end{aligned}$$

the stat variables at time $[n+1]$ are:

$$x_1[n+1] = x_2[n] \tag{5A}$$

$$\begin{aligned} x_2[n+1] = x_2[n] - \frac{Lm}{L} x_1[n] - \frac{T_{period}}{L} x_3[n] + \frac{Lm}{L} I_{ref}[n+1] \\ + \frac{T_{period}}{L}\left(4V_{grid}[n-1] - 2V_{grid}[n-2] - V_{grid-av}[n]\right) \end{aligned} \tag{6A}$$

$$x_3[n+1] = -\frac{Lm}{T_{period}} x_1[n] - x_3[n] + \frac{Lm}{T_{period}} I_{ref}[n+1] + 4V_{grid}[n-1] - 2V_{grid}[n-2] \tag{7A}$$

The state equations give the close loop system as:

$$\begin{bmatrix} I_{load}[n] \\ I_{load}[n+1] \\ V_{op-av}[n] \end{bmatrix} = \begin{bmatrix} 0 & 1 & 0 \\ -\frac{Lm}{L} & 1 & -\frac{T_p}{L} \\ -\frac{Lm}{T_p} & 0 & -1 \end{bmatrix} \begin{bmatrix} I_{load}[n-1] \\ I_{load}[n] \\ V_{op-av}[n-1] \end{bmatrix} + \begin{bmatrix} 0 & 0 & 0 & 0 \\ \frac{Lm}{L} & \frac{4T_p}{L} & -\frac{2T_p}{L} & -\frac{T_p}{L} \\ \frac{Lm}{T_p} & 4 & -2 & 0 \end{bmatrix} \begin{bmatrix} I_{ref}[n+1] \\ V_{grid}[n-1] \\ V_{grid}[n-2] \\ V_{grid-av}[n] \end{bmatrix} \tag{8A}$$

Appendix B: Derivation of Equation (3.32)

the average grid voltage given as:

$$V_{grid-av}[n] = \frac{3}{2}V_{grid}[n] - \frac{1}{2}V_{grid}[n-1] \quad (1B)$$

The controller calculate the average inverter output voltage as

$$V_{op-av}[n] = V_{grid-av}[n] + Lm\frac{I_{ref}[n+1] - I_{load}[n]}{T_{period}}$$

(2B)

The actual inverter current at time $[n+1]$ given as:

$$I_{load}[n+1] = I_{load}[n] + \frac{T_{period}}{L}\left(V_{op-av}[n] - V_{grid-av}[n]\right) \quad (3B)$$

Substitute (2B) in (3B) give:

$$I_{load}[n+1] = \Delta_L\ I_{load}[n] + (1-\Delta_L)\ I_{ref}[n+1] \quad (4B)$$

where $\Delta_L = 1 - \frac{Lm}{L}$

The state variables are:

$$x_1[n] = I_{load}[n]$$
$$x_2[n] = V_{op-av}(n-1)$$

the stat variables at time $[n+1]$ are:

$$x_1[n+1] = \Delta_L\ I_{load}[n] + (1-\Delta_L)\ I_{ref}[n+1] \quad (5B)$$

$$x_2[n+1] = \frac{3}{2}V_{grid}[n] - \frac{1}{2}V_{grid}[n-1] + Lm\frac{I_{ref}[n+1] - I_{load}[n]}{T_{period}} \quad (6B)$$

The state equations give the close loop system as:

$$\begin{bmatrix} I_{load}[n+1] \\ V_{op-av}[n] \end{bmatrix} = \begin{bmatrix} \Delta_L & 0 \\ -\frac{Lm}{T_p} & 0 \end{bmatrix} \begin{bmatrix} I_{load}[n] \\ V_{op-av}[n-1] \end{bmatrix} + \begin{bmatrix} 0 & 0 & 1-\Delta_L \\ -\frac{1}{2} & \frac{3}{2} & \frac{Lm}{T_p} \end{bmatrix} \begin{bmatrix} V_{grid}[n-1] \\ V_{grid}[n] \\ I_{ref}[n+1] \end{bmatrix} \quad (7B)$$

Appendix C: Matlab codes

Traditional control with linear extrapolation

```
clear all;
close all
Vgrms= 240;           %grid rms voltage=240v
Vgm=sqrt(2)*(Vgrms); % Vgm= peak grid voltage
P=10e3;               %inverter power=10KW
Im=(P/Vgrms)*sqrt(2);%Im=inverter peak current
Vdc=400;              %DC link voltage
L=0.002;               %filter inductor value=2mH
Lm=1.8*L;
F=60;                 %grid frequency=60Hz
W = 2*pi*F;           %grid angular frequency
Fs=10e3;              %Fs=sampling frequency=10KHz
Ts=1/Fs;
Tp=Ts;
Ws=W*Ts;              %Discrete time frequency
nmax=499;
n=1:nmax+1;
Vg=Vgm*sin(n*Ws)+0.0*Vgm*sin(5*n*Ws);   %Measured grid voltage
Iref=Im*sin(n*Ws);    %reference inverter current

Il(1)=0 ;   Il(2)=0 ;  Il(3)=0 ; Vop_av(1)=0  ;   Vop_av(2)=0 ;

k=1; Vop_av(3)=0 ;Il(4)=0;
Vmax=400;
s=0;
for  n=4:nmax
Vgav(n)=(5*Vg(n-1)-3*Vg(n-2))/2;
Vop_av(n)=4*Vg(n-1)-2*Vg(n-2)-Vop_av(n-1)+(Lm/Tp)*(Iref(n+1)-Il(n-
1));
if abs(Vop_av(n))>Vmax

 Vop_av(n)=Vop_av(n)*(Vmax/abs(Vop_av(n)));
  else
   end
  u=Vop_av(n)/Vdc;
  um(n)=u;
  uc(n)=abs(u);

  t1=(Ts/2)*(1-abs(u));
  t2=t1;
  Tpw=Ts*abs(u);
  tp(k)=n*Ts;
  tp(k+1)=tp(k)+t1;
  tp(k+2)=tp(k+1)+Tpw;

  Ilp(k)=Il(n);
  Ilp(k+1)=Ilp(k)+(t1/L)*(-Vgav(n));
  Ilp(k+2)=Ilp(k+1)+(Tpw/L)*((u/abs(u))*Vdc-Vgav(n));
  Ilp(k+3)=Ilp(k+2)+(t2/L)*(-Vgav(n));

  Il(n+1)=Ilp(k+3);
  k=k+3;
end
n=[1:nmax];
n=n*1500/500;
```

```
 n1cy=Fs/F;
 n0c=(nmax+1)/n1cy;
 n2=n*(n0c/60)/(3*nmax+1);
 plot(n2,Vop_av,'b')
grid;

s_tp=size(tp);
s_Ilp=size(Ilp);
ms=min([s_tp(2) s_Ilp(2)]);
Ilp=Ilp(1:ms);
tp=tp(1:ms);

te=[0 Ts 2*Ts 3*Ts];
 tp=[te tp];
 Ie=[0 0 0 0];
 Ilp=[Ie Ilp];

hold on
tpp=1:numel(tp);
tpp=tpp*(n0c/60)/(3*nmax+1);

plot(tp,Ilp,'r')
t=tp;
%-------------------------------------------------------------------------
--
% Plotting three-level PWM inverter voltage
dt=1.e-06;
dc=2*dt/Ts;
Kc=floor(1/dc);
for k=1:2*Kc
    if k<= (Kc+1)
        c(k)=1-(k-1)*dc;
    else
        c(k)=(k-Kc-1)*dc;
    end
end
% Generate all pulses in [0 Ts] frame
for kp=1:nmax
    for k=1:2*Kc
        if abs(um(kp)) <= c(k)
           p(kp,k)=0.;
        else
           p(kp,k)=1.;
        end
        if um(kp)<=0
            p(kp,k)=-p(kp,k);
        end
    end
end
% Global time variable
Ks=2*Kc*nmax;
k=1:Ks;
ts=k*dt;
Tm=max(ts);
Vi=Vdc*reshape(p',1,Ks);
n3=[1:nmax+1];
E=Iref-Il;
   hold on
figure(12)
plot(n3,E)
grid;
```

```
hold on
figure(33)
n=1:nmax+1;
plot(n,Vg,n,Il)
grid;
```

%%%%%%%%%%%%%%%%%%%%%%%%%%%%%

Improved control with linear extrapolation

```
clear all;
close all
Vgrms= 240;           %grid rms voltage=240v
Vgm=sqrt(2)*(Vgrms); % Vgm= peak grid voltage
P=10e3;               %inverter power=10KW
Im=(P/Vgrms)*sqrt(2);%Im=inverter peak current
Vdc=400;              %DC link voltage
L=0.002;               %filter inductor value=2mH
Lm=1.8*L;
F=60;                 %grid frequency=60Hz
W = 2*pi*F;           %grid angular frequency
Fs=10e3;              %Fs=sampling frequency=10KHz
Ts=1/Fs;
Tp=Ts;
Ws=W*Ts;              %Discrete time frequency
nmax=499;
n=1:nmax+1;
Vg=Vgm*sin(n*Ws)+0.0*Vgm*sin(5*n*Ws);   %Measured grid voltage
Iref=Im*sin(n*Ws);    %reference inverter current

Il(1)=0 ;   Il(2)=0 ;  Il(3)=0 ; Vop_av(1)=0  ;   Vop_av(2)=0 ;

k=1; Vop_av(3)=0 ;Il(4)=0;
Vmax=400;
s=0;
for  n=4:nmax
Vgav(n)=(5*Vg(n-1)-3*Vg(n-2))/2;
Vop_av(n)=4*Vg(n-1)-2*Vg(n-2)-Vop_av(n-1)+(Lm/Tp)*(Iref(n+1)-Il(n-
1));
if abs(Vop_av(n))>Vmax

 Vop_av(n)=Vop_av(n)*(Vmax/abs(Vop_av(n)));
  else
   end
  u=Vop_av(n)/Vdc;
  um(n)=u;
  uc(n)=abs(u);

  t1=(Ts/2)*(1-abs(u));
  t2=t1;
  Tpw=Ts*abs(u);
  tp(k)=n*Ts;
  tp(k+1)=tp(k)+t1;
  tp(k+2)=tp(k+1)+Tpw;

  Ilp(k)=Il(n);
  Ilp(k+1)=Ilp(k)+(t1/L)*(-Vgav(n));
  Ilp(k+2)=Ilp(k+1)+(Tpw/L)*((u/abs(u))*Vdc-Vgav(n));
  Ilp(k+3)=Ilp(k+2)+(t2/L)*(-Vgav(n));
```

```
  Il(n+1)=Ilp(k+3);
  k=k+3;
end
n=[1:nmax];
n=n*1500/500;
 n1cy=Fs/F;
 n0c=(nmax+1)/n1cy;
 n2=n*(n0c/60)/(3*nmax+1);
 plot(n2,Vop_av,'b')
grid;

s_tp=size(tp);
s_Ilp=size(Ilp);
ms=min([s_tp(2) s_Ilp(2)]);
Ilp=Ilp(1:ms);
tp=tp(1:ms);

te=[0 Ts 2*Ts 3*Ts];
 tp=[te tp];
 Ie=[0 0 0 0];
 Ilp=[Ie Ilp];

hold on
tpp=1:numel(tp);
tpp=tpp*(n0c/60)/(3*nmax+1);

plot(tp,Ilp,'r')
t=tp;
%-------------------------------------------------------------------------
--
% Plotting three-level PWM inverter voltage
dt=1.e-06;
dc=2*dt/Ts;
Kc=floor(1/dc);
for k=1:2*Kc
    if k<= (Kc+1)
        c(k)=1-(k-1)*dc;
    else
        c(k)=(k-Kc-1)*dc;
    end
end
% Generate all pulses in [0 Ts] frame
for kp=1:nmax
    for k=1:2*Kc
        if abs(um(kp)) <= c(k)
           p(kp,k)=0.;
        else
           p(kp,k)=1.;
        end
        if um(kp)<=0
            p(kp,k)=-p(kp,k);
        end
    end
end
% Global time variable
Ks=2*Kc*nmax;
k=1:Ks;
ts=k*dt;
Tm=max(ts);
```

```
Vi=Vdc*reshape(p',1,Ks);
n3=[1:nmax+1];
E=Iref-Il;
   hold on
figure(12)
plot(n3,E)
grid;
hold on
figure(33)
n=1:nmax+1;
plot(n,Vg,n,Il)
grid;
%%%%%%%%%%%%%%%%%%%%%%%%%%%%%%%%%%%%%%%%%
```

TPCC With LSWP

```
clear all;
close all
Vgrms= 240;            %grid rms voltage=240v
Vgm=sqrt(2)*(Vgrms); % Vgm= peak grid voltage
P=10e3;                %inverter power=10KW
Im=(P/Vgrms)*sqrt(2);%Im=inverter peak current
Vdc=400;               %DC link voltage
L=0.002;                %filter inductor value=2mH
Lm=1.8*L;
F=60;                  %grid frequency=60Hz
W = 2*pi*F;            %grid angular frequency
Fs=10e3;               %Fs=sampling frequency=10KHz
Ts=1/Fs;
Tp=Ts;
Ws=W*Ts;               %Discrete time frequency
nmax=499;
n=1:nmax+1;
Vg=Vgm*sin(n*Ws)+0.0*Vgm*sin(5*n*Ws);    %Measured grid voltage
Iref=Im*sin(n*Ws);    %reference inverter current

Il(1)=0 ;    Il(2)=0 ;  Il(3)=0 ; Vop_av(1)=0  ;    Vop_av(2)=0 ;

k=1; Vop_av(3)=0 ;Il(4)=0;
Vmax=400;
s=0;
for  n=4:nmax
 Vgav(n)=(cos(Ws)+(2*(cos(Ws)^2))-.5)*Vg(n-1)-(.5+cos(Ws))*Vg(n-2);
 Vop_av(n)= Vgav(n)+(Lm/Tp)*(Iref(n+1)-Il(n-1))-Vop_av(n-
1)+(cos(Ws)+(2*(cos(Ws)^2))-.5)*Vg(n-2)-(.5+cos(Ws))*Vg(n-3);
 1));
if abs(Vop_av(n))>Vmax

 Vop_av(n)=Vop_av(n)*(Vmax/abs(Vop_av(n)));
  else
   end
  u=Vop_av(n)/Vdc;
  um(n)=u;
  uc(n)=abs(u);

  t1=(Ts/2)*(1-abs(u));
  t2=t1;
  Tpw=Ts*abs(u);
  tp(k)=n*Ts;
  tp(k+1)=tp(k)+t1;
```

```
  tp(k+2)=tp(k+1)+Tpw;

  Ilp(k)=Il(n);
  Ilp(k+1)=Ilp(k)+(t1/L)*(-Vgav(n));
  Ilp(k+2)=Ilp(k+1)+(Tpw/L)*((u/abs(u))*Vdc-Vgav(n));
  Ilp(k+3)=Ilp(k+2)+(t2/L)*(-Vgav(n));

  Il(n+1)=Ilp(k+3);
  k=k+3;
end
n=[1:nmax];
n=n*1500/500;
 n1cy=Fs/F;
 n0c=(nmax+1)/n1cy;
 n2=n*(n0c/60)/(3*nmax+1);
 plot(n2,Vop_av,'b')
grid;

s_tp=size(tp);
s_Ilp=size(Ilp);
ms=min([s_tp(2) s_Ilp(2)]);
Ilp=Ilp(1:ms);
tp=tp(1:ms);

te=[0 Ts 2*Ts 3*Ts];
 tp=[te tp];
 Ie=[0 0 0 0];
 Ilp=[Ie Ilp];

hold on
tpp=1:numel(tp);
tpp=tpp*(n0c/60)/(3*nmax+1);

plot(tp,Ilp,'r')
t=tp;
%-------------------------------------------------------------------------
--
% Plotting three-level PWM inverter voltage
dt=1.e-06;
dc=2*dt/Ts;
Kc=floor(1/dc);
for k=1:2*Kc
    if k<= (Kc+1)
        c(k)=1-(k-1)*dc;
    else
        c(k)=(k-Kc-1)*dc;
    end
end
% Generate all pulses in [0 Ts] frame
for kp=1:nmax
    for k=1:2*Kc
        if abs(um(kp)) <= c(k)
           p(kp,k)=0.;
        else
           p(kp,k)=1.;
        end
        if um(kp)<=0
            p(kp,k)=-p(kp,k);
        end
    end
```

```
end
% Global time variable
Ks=2*Kc*nmax;
k=1:Ks;
ts=k*dt;
Tm=max(ts);
Vi=Vdc*reshape(p',1,Ks);
n3=[1:nmax+1];
E=Iref-Il;
   hold on
figure(12)
plot(n3,E)
grid;
hold on
figure(33)
n=1:nmax+1;
plot(n,Vg,n,Il)
grid;
%%%%%%%%%%%%%%%%%%%%%%%%%%%%%%%%%%%%%%
```

IPCC With LSWP

```
clear all;
close all
Vgrms= 240;           %grid rms voltage=240v
Vgm=sqrt(2)*(Vgrms);  % Vgm= peak grid voltage
P=10e3;               %inverter power=10KW
Im=(P/Vgrms)*sqrt(2);%Im=inverter peak current
Vdc=400;              %DC link voltage
L=0.002;               %filter inductor value=2mH
Lm=1.8*L;
F=60;                 %grid frequency=60Hz
W = 2*pi*F;           %grid angular frequency
Fs=10e3;              %Fs=sampling frequency=10KHz
Ts=1/Fs;
Tp=Ts;
Ws=W*Ts;              %Discrete time frequency
nmax=499;
n=1:nmax+1;
Vg=Vgm*sin(n*Ws)+0.0*Vgm*sin(5*n*Ws);   %Measured grid voltage
Iref=Im*sin(n*Ws);   %reference inverter current

Il(1)=0 ;   Il(2)=0 ;  Il(3)=0 ; Vop_av(1)=0  ;   Vop_av(2)=0 ;

k=1; Vop_av(3)=0 ;Il(4)=0;
Vmax=400;
s=0;
for  n=4:nmax
 Vgav(n)=(.5*Vg(n))+((cos(Ws))*Vg(n))-(.5*Vg(n-1));

 Vop_av(n)=Vgav(n)+(Lm/Tp)*(Iref(n+1)-Il(n));

if abs(Vop_av(n))>Vmax

 Vop_av(n)=Vop_av(n)*(Vmax/abs(Vop_av(n)));
  else
   end
  u=Vop_av(n)/Vdc;
  um(n)=u;
  uc(n)=abs(u);
```

```
  t1=(Ts/2)*(1-abs(u));
  t2=t1;
  Tpw=Ts*abs(u);
  tp(k)=n*Ts;
  tp(k+1)=tp(k)+t1;
  tp(k+2)=tp(k+1)+Tpw;

  Ilp(k)=Il(n);
  Ilp(k+1)=Ilp(k)+(t1/L)*(-Vgav(n));
  Ilp(k+2)=Ilp(k+1)+(Tpw/L)*((u/abs(u))*Vdc-Vgav(n));
  Ilp(k+3)=Ilp(k+2)+(t2/L)*(-Vgav(n));

  Il(n+1)=Ilp(k+3);
  k=k+3;
end
n=[1:nmax];
n=n*1500/500;
 n1cy=Fs/F;
 n0c=(nmax+1)/n1cy;
 n2=n*(n0c/60)/(3*nmax+1);
 plot(n2,Vop_av,'b')
grid;

s_tp=size(tp);
s_Ilp=size(Ilp);
ms=min([s_tp(2) s_Ilp(2)]);
Ilp=Ilp(1:ms);
tp=tp(1:ms);

te=[0 Ts 2*Ts 3*Ts];
 tp=[te tp];
 Ie=[0 0 0 0];
 Ilp=[Ie Ilp];

hold on
tpp=1:numel(tp);
tpp=tpp*(n0c/60)/(3*nmax+1);

plot(tp,Ilp,'r')
t=tp;
%-------------------------------------------------------------------
--
% Plotting three-level PWM inverter voltage
dt=1.e-06;
dc=2*dt/Ts;
Kc=floor(1/dc);
for k=1:2*Kc
    if k<= (Kc+1)
        c(k)=1-(k-1)*dc;
    else
        c(k)=(k-Kc-1)*dc;
    end
end
% Generate all pulses in [0 Ts] frame
for kp=1:nmax
    for k=1:2*Kc
        if abs(um(kp)) <= c(k)
           p(kp,k)=0.;
        else
```

```
            p(kp,k)=1.;
        end
        if um(kp)<=0
            p(kp,k)=-p(kp,k);
        end
    end
end
% Global time variable
Ks=2*Kc*nmax;
k=1:Ks;
ts=k*dt;
Tm=max(ts);
Vi=Vdc*reshape(p',1,Ks);
n3=[1:nmax+1];
E=Iref-Il;
   hold on
figure(12)
plot(n3,E)
grid;
hold on
figure(33)
n=1:nmax+1;
plot(n,Vg,n,Il)
grid;
```